

Substrate Integrated Coaxial Line based Bandpass Filters

Design of efficient microwave/millimeter components has become very much pertinent to implementation of high capacity and low latency wireless system. To accommodate the steady inception of newly emerging applications such as FR-2 5G telephony, collision avoidance radar for self-driven cars, passive millimeter wave imaging, 802.11 ad WLAN, the millimeter-wave portion of the electromagnetic spectrum is proposed to be utilized [180]. For the coexistence of mm-wave applications with better signal to noise ratio (SNR), it is essential to have highly selective bandpass filters with good out of the band rejection. Design of bandpass filter at millimeter-wave range poses challenges of attaining low-insertion loss & high selectivity with good integration capability. Therefore microwave/ millimeter-wave filters attracts significant attention in building the modern transceiver system. Several technologies to implement bandpass filters for millimeter front-end system have been tried previously. Microstrip technology enjoys advantages like low profile and good integration ability. However, they are not preferable for operation in millimeter frequency range due to radiation loss and surface wave loss at high frequency. The oldest yet effective solution for design of microwave/millimeter filter in satellite communication has been waveguide based filters due to their high Q-factor, low loss, and high stability to environmental factors. But, the merits of traditional waveguide based components are limited for using in bulky systems and cannot be implemented in portable handheld equipment. The advancements in PCB technology enabled building waveguides on low profile substrates, namely, substrate integrated waveguide (SIW) technology [181]. The self-shielded and planar form factor of SIW makes it a appealing substitute of metallic waveguides to design of bandpass filters with high Q-factor at millimeter-wave frequency bands. However, utilization of SIW is limited as it occupies larger area than TEM based circuits and cannot offer broad-bandwidth due to its inherent narrow mono-mode bandwidth. Furthermore, the upcoming 5G wireless standards will require circuits to simultaneously operate at microwave and millimeter-wave frequency bands. SICL technology is an excellent choice to realize such circuits as the previously discussed microstrip and SIW technologies face various challenges in realizing widely spaced passbands for dual-bandpass operation at millimeter-wave bands.

This chapter deals with the design and development of compact SICL based bandpass-filters with the help of proposed novel design techniques. In the first design, a dual-mode bandpass filter is realized by exciting the degenerate modes in a novel square-shaped SICL cavity filter. A cross-shaped slot etched on the middle square patch provides wider bandwidth by combining the two higher order modes and enhances the frequency selectivity by a transmission zero on the upper side of passband. Further size reduction of SICL cavity is achieved by modeling a L-bend SICL line confined between a pair of dielectrics and shorted at both ends to via-wall. A dual-mode bandpass filter is devised by coupling a pair of half-mode cavities generated from the proposed SICL cavity. In the designed bandpass filter, the selectivity is improved by creating a pair of transmission zeros on each lower and upper side of the passband. The third filter design proposed in this chapter leverages a dual-bandpass operation in an SICL cavity with L-shaped slots etched on diagonally opposite ends of a square patch. A fully shielded compact dual-mode dual-band filter is realized by coupling two quarter-mode cavities of this proposed SICL-cavity supporting TEM and TE_{110} mode of propagation in the lower and upper passband, respectively. The next work in this chapter deals with the design of a self-packaged highly selective bandpass filter with for K_u band

using a ring resonator with a novel perturbation technique. The proposed perturbation technique devised by changing the width of outer conductor formed by lateral vias for the first time could successfully vary the characteristic impedance of an SICL section. Contrary to realizing coaxial filters in multi-layered substrates, a single layered wide-band filter with TEM based planar coaxial resonators is proposed. This single-layered bandpass filter is conceived by merging *TEM* based modes of two SICR and *TE*₁₀₁ mode by SIW also features high degree of flexibility in positioning the transmission zeros to improve the selectivity as well as extend the out-of-band rejection. All designs are fabricated and validated by experimental results.

3.1 DUAL-MODE SICL BANDPASS FILTER WITH A NOVEL PERTURBED OUTER CONDUCTOR FOR *K_U*-BAND

K_u-band has been a preferred choice to host satellite (very small aperture terminals) and RADAR communication [19]. While designing a bandpass filter for *K_u*-band it becomes increasingly important to model low-loss compact filter with high-selectivity to reduce the guard-band for better utilization of available spectrum. A novel SICL based bandpass filter is realized by exciting the even and odd modes in an SICL ring resonator. A novel perturbation technique to control the coupling between orthogonal modes is realized by varying the width of the outer conductor formed by metallic vias in this planar coaxial line. So far in literature, the lateral metalized vias in SICL based circuits are utilized to reduce crosstalk and form a shielded structure to minimize radiation loss. In the following work, for the first time to the best of knowledge, the characteristic impedance of SICL section could be successfully varied by changing the width of outer conductor formed by lateral vias. Further, the effect of perturbation length and inset on resonant frequency and attenuation pole is studied. The two transmission zeros produced close to the pass band provide excellent selectivity and reject spurious frequencies up to $1.9f_o$. The proposed SICL based filter is manufactured using low cost PCB fabrication process.

3.1.1 Configuration of dual-mode SICL bandpass filter and analysis

The geometry of the proposed filter is shown in Fig. 3.1(a). It comprises of a ring-shaped uniform impedance resonator (UIR) sandwiched between two dielectric substrates. A series of lateral metallic vias enclosing the UIR along with bottom and top ground plane form outer conductor of this planar dielectric filled coaxial line. Further, the spacing and pitch of vias are chosen such that the electromagnetic wave leakage is minimal. The first four resonant modes in an SICL resonator are a pair of degenerate $TM_{110(\text{even,odd})}$ and $TM_{210(\text{even,odd})}$ modes as depicted in Fig. 3.2. The one-wavelength long SICL ring resonator is capacitively fed by SICL section having both its ports separated by $\lambda_g/4$ section between them. A perturbation is devised at a distance $3\lambda_g/8$ from the feeding point by offsetting series of vias from their original contour to design the proposed dual-mode bandpass filter. The length of this perturbation is L_p and depth of inset is denoted by R_2 as shown in Fig. 3.1(a). In [51], the characteristic impedance (Z_o) of SICL is considered as a function of width of inner conductor and thickness of dielectric substrate. Also in earlier reported works change in position of lateral vias has not shown any significant variation in characteristic impedance of SICL [7]. In this work, for the first time it is shown that Z_o of SICL can be perturbed varying the position of lateral vias by maintaining small width of inner conductor to height of substrate ($W_{in}/2H$) ratio. In the proposed design a planar coaxial line (SICL) is modeled using a conducting strip and series of delimiting vias acting as inner and outer conductor respectively. Due to the change in width of the outer conductor, the characteristic impedance of SICL section is changed over the length L_p , forming a coaxial stepped impedance resonator in planar form. Variation in characteristic impedance of the perturbed section (Z_p) with change in perturbation inset is recorded in Fig. 3.3(a) using Ansys HFSS full-wave simulator. Further, the characteristic impedance of unperturbed section is denoted by Z_r . However, the variation in

impedance of perturbed section is limited by thickness of the substrate and fabrication tolerance. This perturbation leads to excitation of even and odd mode in the SICL based ring resonator which can be controlled by inset of perturbation as observed from Fig. 3.3(b). One of the distinctive advantages of using TEM based SICL technology over SIW for higher frequencies is along with

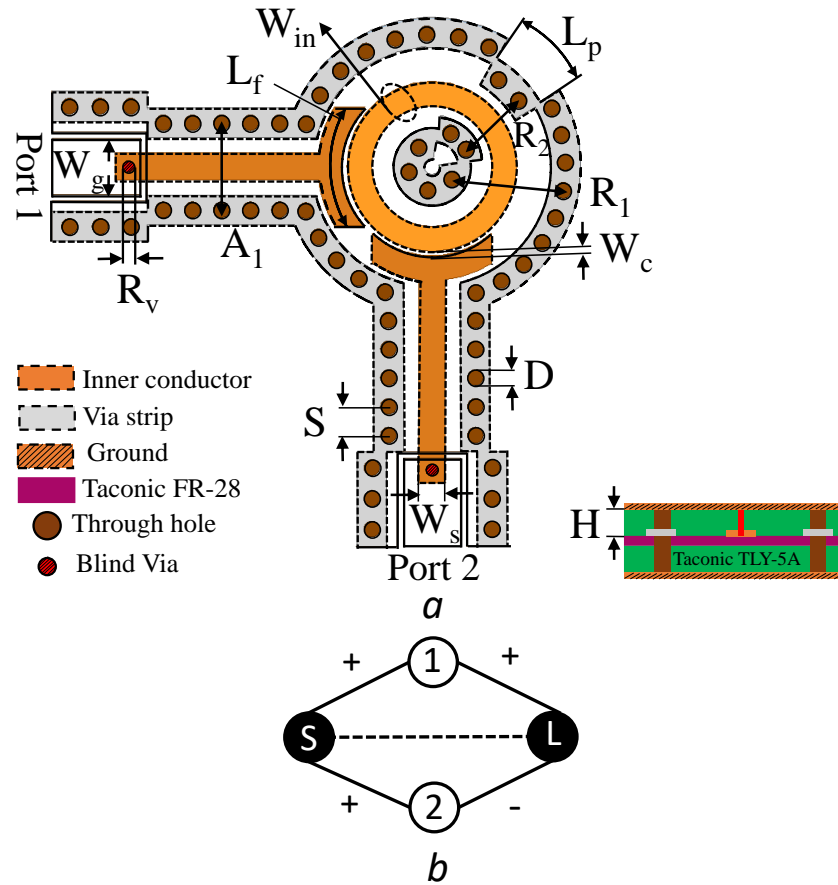


Figure 3.1: Proposed dual-mode SICL bandpass filter for K_u band (a) Geometrical layout with dimensions: $A_1 = 2.75\text{mm}$, $D = 0.5\text{mm}$, $L_f = 4.03\text{mm}$, $L_p = 1.97\text{mm}$, $S = 0.92\text{mm}$, $R_1 = 3.5\text{mm}$, $R_2 = 2.26\text{mm}$, $R_v = 0.36\text{mm}$, $W_c = 0.14\text{mm}$, $W_g = 1.78\text{mm}$, $W_{in} = 0.78\text{mm}$, $W_s = 0.85\text{mm}$ (b) Coupling scheme

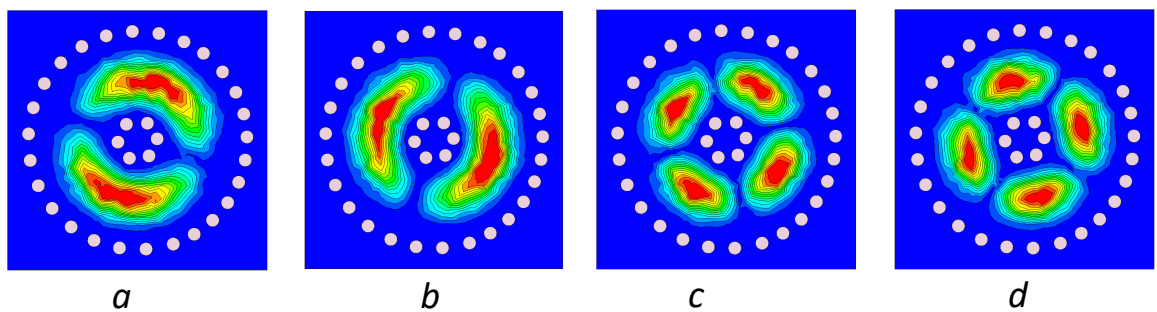


Figure 3.2: Magnitude of electric field distribution in an SICL ring resonator (a) TM_{110} (Even mode) (b) TM_{110} (Odd mode) (c) TM_{210} (Even mode) (d) TM_{210} (Odd mode)

low loss shielded nature, first two modes are the degenerate modes and higher order modes are about $2f_o$ apart from fundamental mode to provide broad out of band suppression without any additional complexity in the circuit. Since the higher order mode frequency is dependent on the impedance ratio R_z (where $R_z = Z_p/Z_r$), the higher order mode can be further shifted by realizing smaller value of Z_p using the proposed perturbation inset R_2 . The coupling between the even and odd mode resonance can be controlled by depth of inset (R_2) as well as length of perturbation (L_p) as shown by the computed coupling coefficients [80] in Fig. 3.4. The proposed dual-mode filter is synthesized with the help of coupling matrix developed from the coupling scheme shown in Fig. 3.1(b). The dual-mode filter designed using the even and odd TM_{110} modes has center frequency at 13.85 GHz, with a fractional bandwidth (FBW) of 2.6% and transmission zeros at 13.05 GHz and 15.03 GHz as shown in Fig. 3.5. The self resonance frequency of even mode under perturbation is less than odd mode as observed from Fig. 3.3 (b). Hence M_{11} is smaller than M_{22} and the transmission zero due to interaction of orthogonal modes occurs on the lower side of the passband

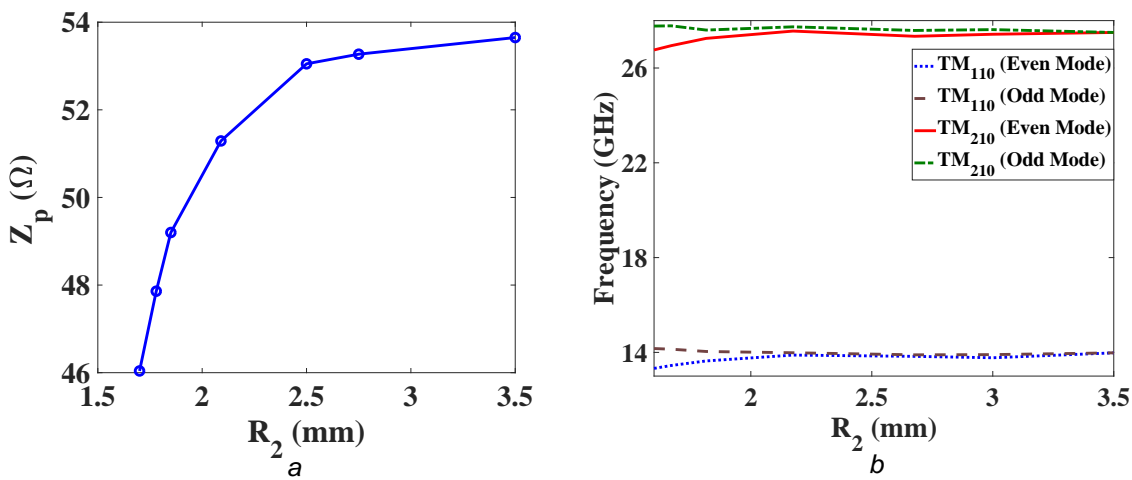


Figure 3.3 : Effect of perturbation inset (R_2) on: (a) Characteristic impedance of perturbed section (b) Resonant modes

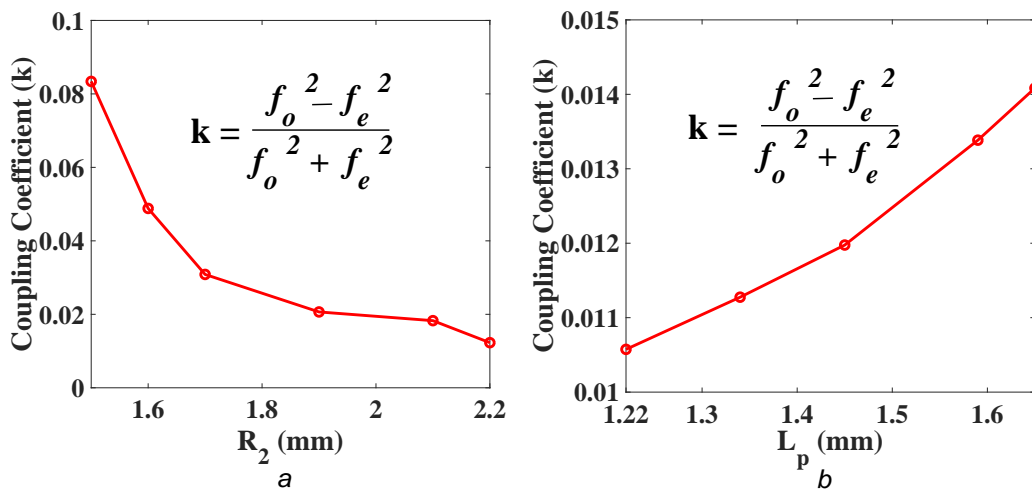


Figure 3.4 : Computation of coupling coefficient (k) between even and odd modes as a function of: (a) Perturbation inset (R_2) (b) Perturbation length (L_p)

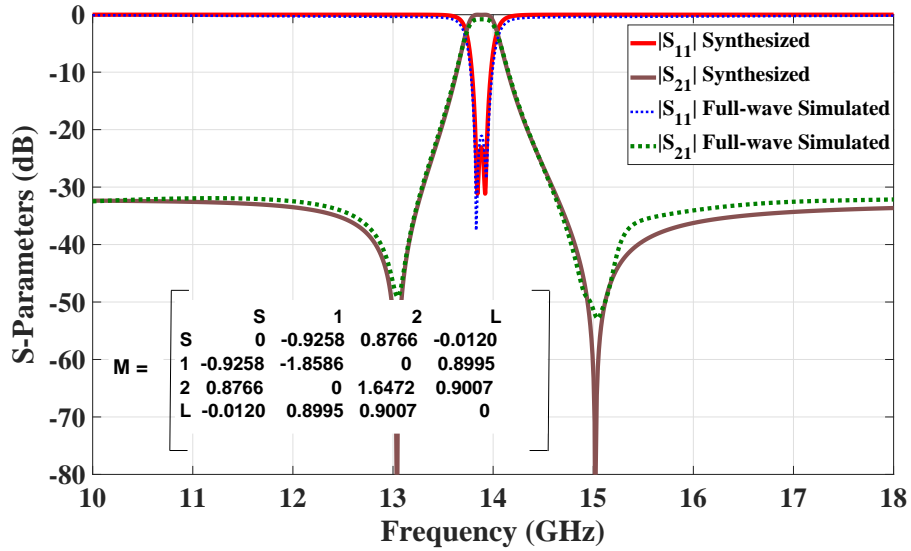


Figure 3.5 : Filter response generated using coupling matrix and the full-wave simulated S-parameters

[77]. Further, the C-shaped feed lines capacitively coupled to the SICL ring resonator facilitates source to load coupling to create a transmission zero on upper side of the passband as shown in Fig. 3.5. The two transmission zeros not only provide sharp rejection to the filter but also aid in deep spurious signal suppression of better than 30 dB on lower and upper side of the passband. In Fig. 3.6(a), it is observed as the length of perturbation is reduced the transmission zeros move closer to the passband. Now to illustrate the role of outer conductor formed by lateral vias in this planar coaxial filter R_1 is varied as shown in Fig. 3.6(b). The position of transmission zeros change with variation in R_1 and when $R_1 > 2\text{mm}$ (with corresponding $R_z > 1$) the transmission zeros do not occur as shown in Fig. 3.6(b). Further to affirm the significance of the proposed perturbation the performance of filter with perturbation ($R_1 = 3.5\text{mm}$ and $R_2 = 2.26\text{mm}$) and without perturbation ($R_1 = R_2 = 3.5\text{mm}$) are compared in Fig. 3.7(a). In case of no perturbation, the coupling coefficient between even and odd mode equals to zero as both orthogonal modes occur at same frequency.

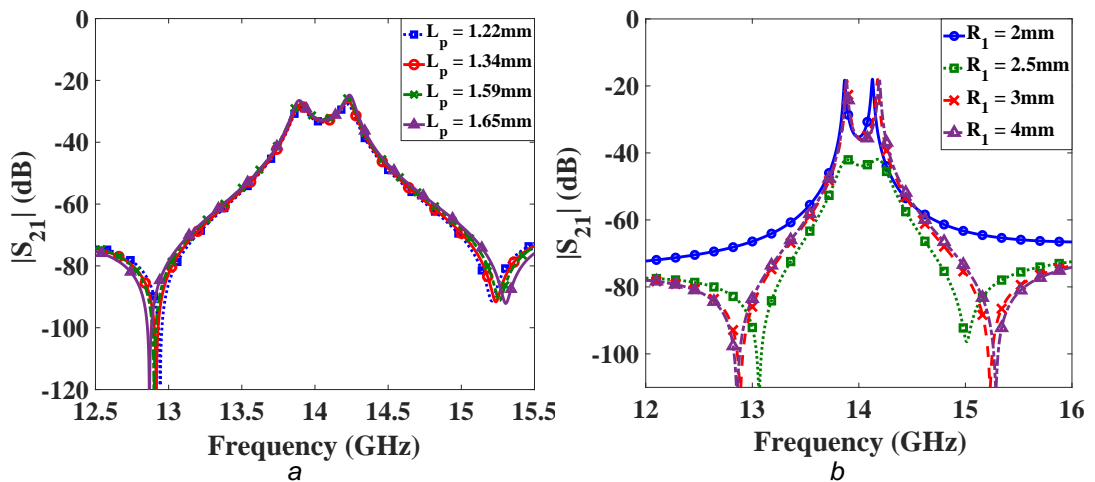


Figure 3.6 : Study of proposed dual-mode SICL based bandpass filter (a) Dependence of transmission zero on perturbation length (L_p) (b) Variation in $|S_{21}|$ due to R_1

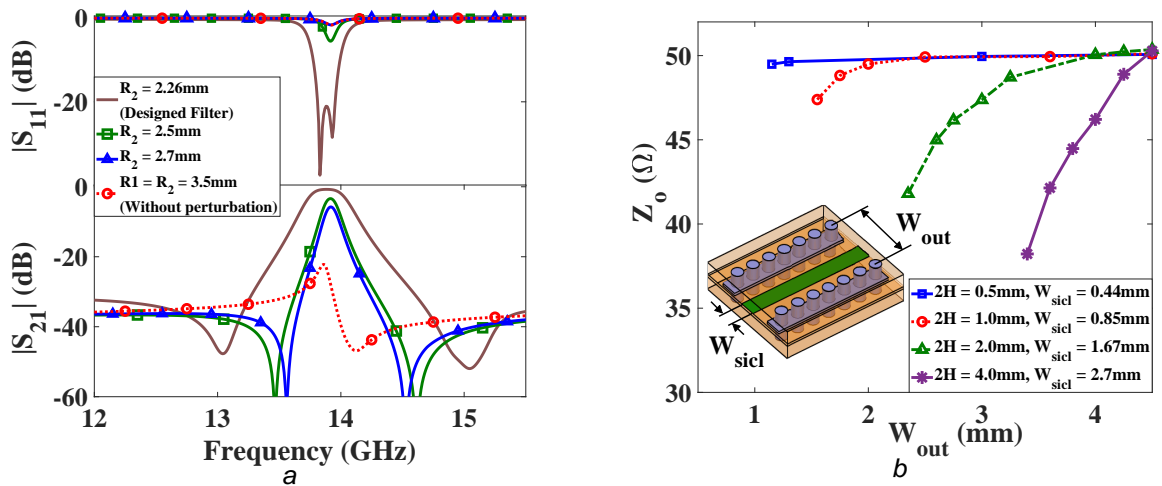


Figure 3.7 : Investigation on (a) Change in perturbation inset (b) Variation in Z_o with change in width of outer conductor (W_{out})

Whereas, the proposed perturbation provides flexibility to design a dual-mode bandpass filter at the desired frequency. The change in Z_o of a 50 Ω SiCL line with variation in spacing between lateral vias (W_{out}) for various substrate height is illustrated in Fig. 3.7(b). It is observed that with increase in substrate height, the range of impedance variation increases with change in W_{out} and width of outer conductor also becomes a prominent factor in deciding the Z_o of SiCL.

3.1.2 Experimental verification and discussion

The proposed SiCL based filter is manufactured using standard multilayer PCB fabrication technology involving drilling, electroplating and etching. A pair of Taconic TLY-5A ($\epsilon_r = 2.2$, $\delta = 0.0009$) substrate, each of thickness 0.508 mm is bonded using Taconic FR-28 prepreg ($\epsilon_r = 2.74$, $\tan\delta = 0.0014$) of 4 mil thickness. The photograph of the fabricated prototype depicting its top and bottom view is shown in Fig. 3.8. To facilitate measurement of the proposed filter, SiCL to GCPW transitions have been used at both the ports. The full-wave S-parameters obtained through Ansys HFSS are validated by experimental results recorded using Agilent N5234A network analyzer

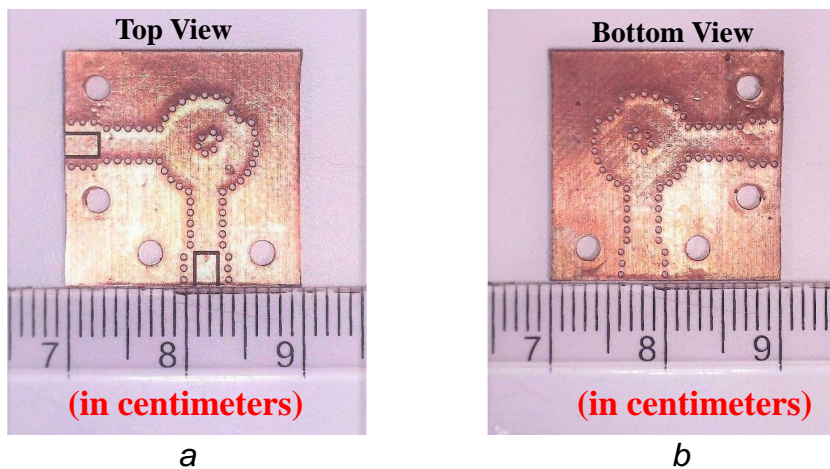


Figure 3.8 : Photograph of the fabricated prototype (a) Top view (b) Bottom view

Table 3.1: Comparison of proposed SICL filter with earlier reported filters

Ref	Tech.	f_o (GHz)	Order	$ S_{21} $ (dB)	Selectivity (L_L/L_U)	Size (λ_g^2)	Shielded	Self packaged
[74]	LTCC	14.52	2	3.27	N.M	0.37	No	Yes
	MS	13.2	5	1.75	0.8/ 0.75	0.11	No	No
	SIW	13.06	5	1.96	0.33/ 0.603	1.48	Yes	Yes
[21]	MS	13.31	5	2.1	0.95/ 0.823	0.12	No	No
	MS	13.325	5	1.78	2.175/ 1.525	0.06	No	No
[75]	SIW	14.3	3	2.9	N.M	N.M	Yes	Yes
[76]	SIW	14.42	2	2.6	N.M	0.55	Yes	Yes
[79]	ESICL	15	4	1.59	N.M	2.85	Yes	Yes
TW	SICL	13.83	2	1.18	0.31/ 0.46	0.31	Yes	Yes

MS: Microstrip, TW: This work, N.M:Not mentioned, L_L, L_U : Selectivity on lower and upper side of passband respectively.

Note: Filter with better roll-off rate has smaller L_u and L_L

as shown in Fig. 3.9. The proposed filter exhibits a fractional bandwidth of 2.6% with 3-dB passband of 360 MHz centered at 13.83 GHz (f_o). The selectivity of the proposed SICL based filter is enhanced by transmission zeros produced on upper and lower edge of passband at 13.03 and 14.93 GHz, respectively. A stop-band rejection up to 26.2 GHz ($1.9f_o$) is achieved in the proposed SICL based filter. The slight discrepancy between simulated and measured results is attributed to fabrication tolerance and bonding of the multilayer PCB. The performance of the proposed SICL based bandpass filter is compared with the previously reported bandpass filters in Table 3.1. In order to compare the selectivity of the proposed SICL based filter with previously reported K_u -band filters, the formulation used in [21] is considered. The filter with better roll-off rate has smaller L_u

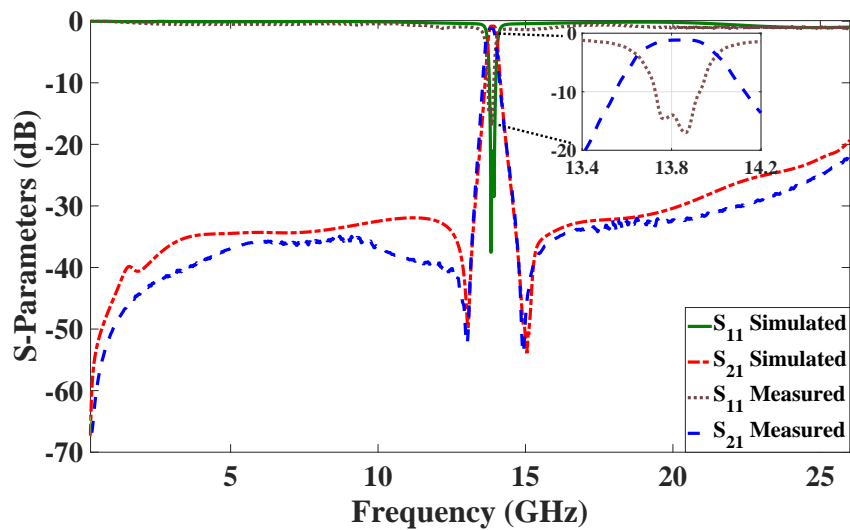


Figure 3.9: Comparison between full-wave simulated and experimental results of the proposed SICL based dual-mode bandpass filter

and L_L . The roll-off rate for a filter can be improved by increasing the order of the filter at the cost of higher insertion loss. In the proposed filter, transmission zeros on lower and upper side of passband of this 2nd order filter provide steeper rejection skirt even as compared to 5th order filters as shown in Table 3.1. Though microstrip based filters demonstrate small size, they have larger insertion loss and cannot be scaled to higher frequency as they are prone to radiation loss due to their semi-open structure. Further, the proposed SICL filter exhibits a compact form factor compared to its shielded counterparts (SIW and ESICL) as shown in Table 3.1.

3.2 DUAL-MODE SICL CAVITY FILTER FOR MILLIMETER-WAVE APPLICATIONS

3.2.1 Modeling of substrate integrated coaxial line cavity

The geometrical layout of the proposed substrate integrated coaxial line (SICL) cavity is shown in Fig. 3.10(a). A square patch of side length around $\lambda_g/2$ is sandwiched between two layers of dielectric substrate, where λ_g is the guided wavelength at design frequency. This configuration is bounded by rows of metallic vias connecting the top and bottom plane which are in contact with one opposite sides of inner conducting patch. The other two sides are kept at G_1 distance from the via row. A metallic strip is enforced through the vias to strengthen the coaxial nature of the designed cavity. Using Ansys HFSS Eigen mode solver the dominant mode and vector electric field is identified. The proposed cavity has a side of length $W_p = 4.95\text{mm}$, that corresponding to nearly $\lambda_g/2$ at 20.5 GHz exhibiting dominant TEM based mode of propagation. The spacing between the vias S and diameter of via D_v are so chosen as to avoid any electromagnetic leakage from the designed SICL cavity. In the above design, $S = 0.9\text{mm}$ and $D = 0.6\text{mm}$. The vector electric field of the proposed square SICL cavity is depicted in 3.10(b). From the radially outward directed vector electric field it is evident that the proposed configuration acts as a coaxial line in printed form. The design of the proposed dual-mode SICL filter starts with modeling of coupling topology. Two SICL 50 Ω arms are inset on short-circuited ends of the SICL cavity. The strength of coupling can be adjusted by the depth (L_{in}) and width of the inset (W_{in}) as shown in Fig. 3.11. The excitation

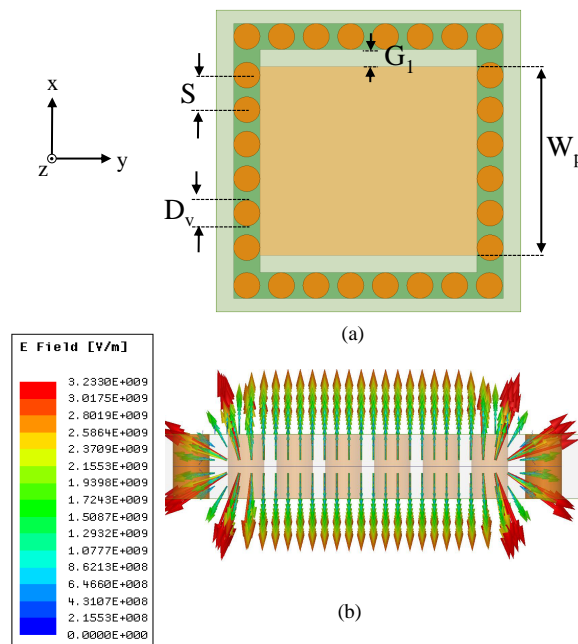


Figure 3.10 : Design of the proposed SICL based cavity (a) Geometrical layout (b) Vector E-field distribution at 20 GHz.

of higher order mode depends on the size of coupling window (A). The SICL cavity with square shaped inner conductor with side length W_p . The inline ports are offset (O_1) from the center of square patch by 0.8mm to adjust the coupling between the higher order modes. The vector electric field of the two higher order orthogonal TM_{120}^z and TM_{210}^z modes occurring at 27.8 GHz and 37.6 GHz are depicted in Fig. 3.12(a) and (b) respectively. A perturbation is created in the designed SICL based cavity to create orthogonal degenerate mode at 28 GHz. The coupling schema of the proposed dual-mode SICL based filter is presented in Fig. 3.13. The two poles generated by the higher order modes resonances are modeled as node 1 and 2 in the coupling topology. By realizing the coupling coefficients as shown in the coupling matrix it is possible to excite the degenerate modes at 28 GHz to realize a two-poles filter with transmission zero on the upper side of the passband. The synthesized coupling matrix given below [52] determines the coupling between the higher order modes to achieve the required filtering function.

$$\begin{bmatrix} & \mathbf{S} & \mathbf{1} & \mathbf{2} & \mathbf{L} \\ \mathbf{S} & 0 & -0.7760 & 1.0676 & 0 \\ \mathbf{1} & -0.7760 & -1.8439 & 0 & 0.7760 \\ \mathbf{2} & 1.0676 & 0 & 1.7582 & 1.0676 \\ \mathbf{L} & 0 & 0.7760 & 1.0676 & 0 \end{bmatrix}$$

To excite the degenerate mode in the proposed SICL cavity, two cross-shaped slots of unequal width and length are etched at the center of a corner cut inner square-shaped conductor of SICL section. The length and width of the slots are carefully adjusted to achieve the desired coupling coefficient as shown in the coupling matrix. The effect on proposed filter performance with

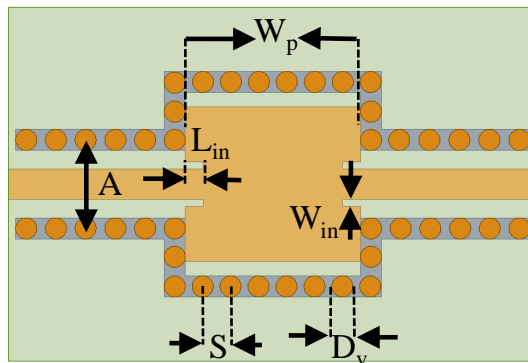


Figure 3.11 : Top view of the proposed center coupled inset fed SICL cavity

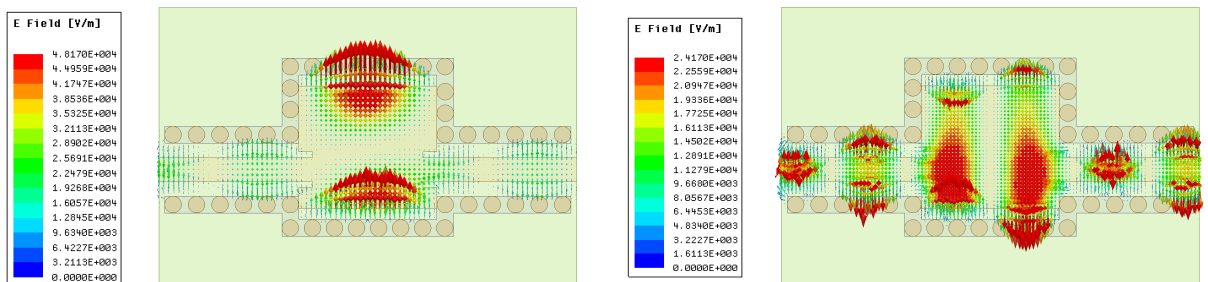


Figure 3.12 : Vector electric field distribution at higher order modes (a) TM_{120}^z mode at 27.8 GHz (b) TM_{210}^z at 37.65 GHz.

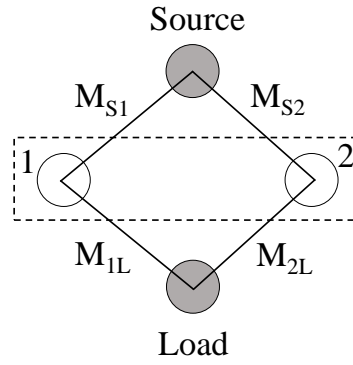


Figure 3.13 : Coupling schema of the proposed SICL based dual-mode filter

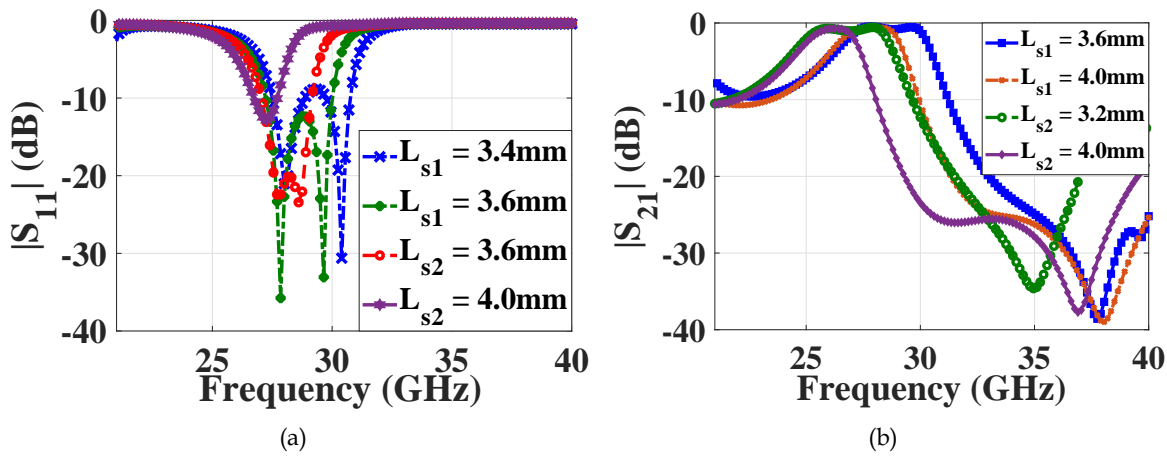


Figure 3.14 : Variation in (a) reflection coefficient and (b) insertion loss with change in slot lengths.

variation in slot length has been studied in Fig. 3.14. The final layout of the proposed dual-mode SICL filter is as portrayed in Fig. 3.15 and dimensions are listed in Table 3.2. By observing the coaxial like radially outward directed E-field vector of proposed SICL dual-mode bandpass filter in Fig. 3.16, it is confirmed that the proposed design is the planar form of traditional coaxial line. The full-wave and the synthesized filter responses are depicted in Fig. 3.17.

3.2.2 Experimental Results & Discussion

The proposed filter synthesis technique is affirmed by fabricating an SICL based dual-mode bandpass filter using a pair of low loss Taconic TLY-5 ($\epsilon_r = 2.2$, $\tan\delta = 0.0009$) substrate each of thickness 0.508 mm, which are bonded using Taconic FR-28 prepreg ($\epsilon_r = 2.74$, $\tan\delta = 0.0014$). The photograph depicting the top and bottom view of the fabricated experimental prototype is shown in Fig. 3.18 (a) & (b). In order to measure the S-parameters of the proposed prototype using a standard vector network analyzer (VNA), a transition is from SICL technology to grounded-coplanar waveguide (GCPW) is devised using a metallic via to connect the conducting middle layer to the central conductor of GCPW. The working principle of the proposed dual-mode SICL based bandpass filter is confirmed by recording the scattering parameters from Agilent N5234A VNA. The measured S-parameters of the designed filter depicted in Fig. 3.18 (c) indicates the center frequency of passband at 28.15 GHz. A roll-off in the upper passband is observed

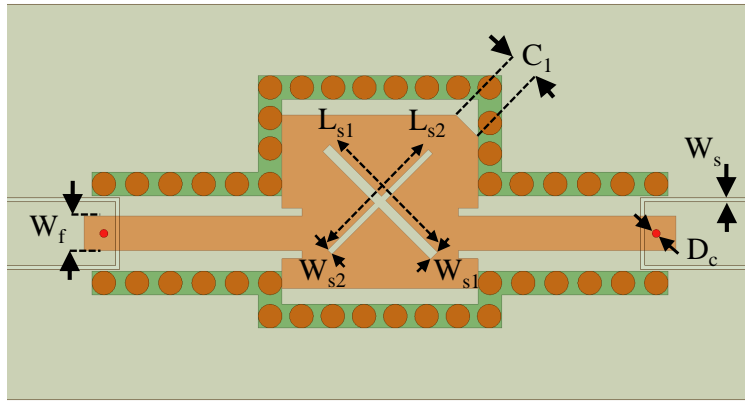


Figure 3.15 : Top view of the proposed dual-mode SICL based filter with dimensions.

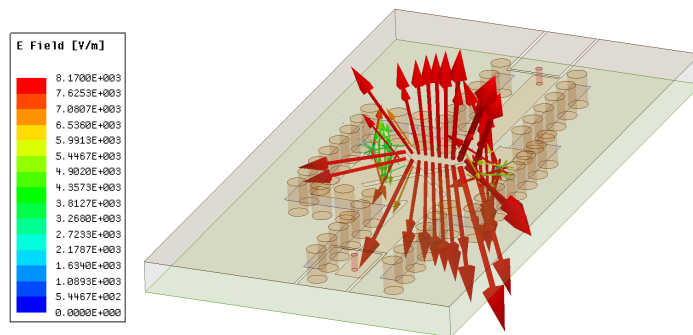


Figure 3.16 : E-field vector plot at 28.25 GHz in the proposed SICL based dual-mode cavity filter

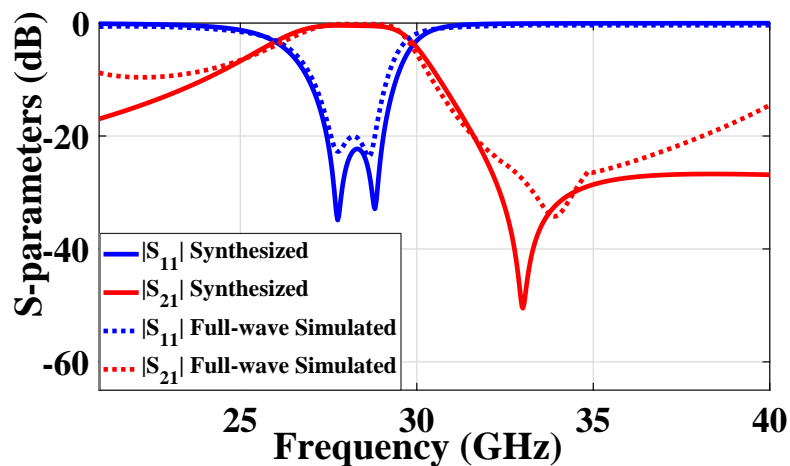


Figure 3.17 : S-Parameters of the synthesized and full-wave simulated dual-mode SICL based bandpass cavity filter

because of the cancellation of fields by the two orthogonal higher order modes. At least 15 dB out of the band rejection is achieved up to 40 GHz. A measured 3-dB passband ranging from 25.8

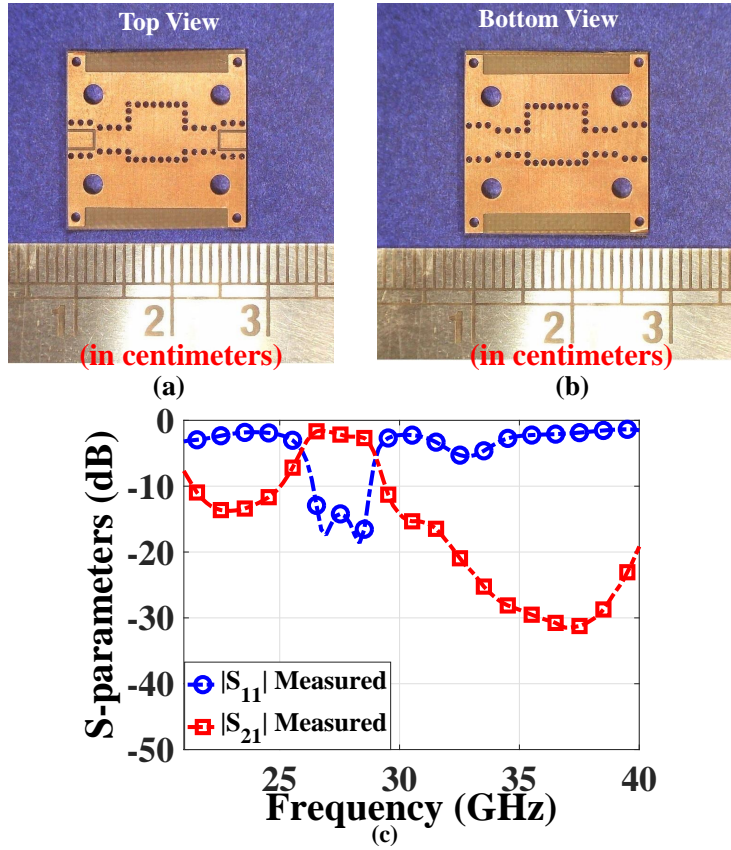


Figure 3.18 : Proposed dual-mode SICL cavity based bandpass filter. Photograph of fabricated prototype of depicting (a) Top view (b) Bottom View (c) Experimentally measured S-parameters of the fabricated prototype.

GHz to 28.93 GHz is observed with an insertion loss of 2.43 dB at the center frequency 27.365 GHz as compared to the 0.42 dB insertion loss in simulation. The deviation observed in measured results is due to fabrication tolerance that plays an significant role at millimeter-wave band. Moreover, the losses due to connector are taken in to account for measured results which have

Table 3.2 : Dimensions of the designed SICL cavity based bandpass filter

Parameter	Value (mm)	Parameter	Value (mm)
W_p	4.95	L_{s1}	3.85
W_{s1}	0.24	L_{s2}	3.6
S	0.9	L_{in}	0.5
W_{s2}	0.15	A	2.4
W_{in}	0.2	D_c	0.2
W_s	0.1	D_v	0.6
W_f	0.87	G_1	0.4
C_1	0.77	O_1	0.8

not been considered in the full-wave simulation. From the Eigen mode solver of HFSS, it is seen that the dominant mode of the bandpass filter shifts down to 17.8 GHz due to external loading and cross-shaped slots. The designed SICL bandpass filter occupies $6.38 \text{ mm} \times 6.14 \text{ mm}$ or equivalently $0.56\lambda_g \times 0.54\lambda_g$, where λ_g is guided wavelength at 17.8 GHz. A SIW cavity designed at the same resonant frequency covers $8.86 \text{ mm} \times 8.31 \text{ mm}$, or equivalently $1.55\lambda_g \times 1.46\lambda_g$ area. Hence, the proposed SICL based cavity filter occupies only 53.2% of area as compared to a SIW cavity.

3.3 DESIGN OF A SUBSTRATE INTEGRATED HALF MODE COAXIAL CAVITY FILTER WITH MULTIPLE TRANSMISSION ZEROS

In the previous section we saw the design and realization of bandpass filter using an SICL cavity that occupies only 53.8% lateral area as compared to an SIW cavity. Another promising technique to design compact filters is to use half-mode SICL cavity. Moreover, utilization of half-mode cavity provides better design flexibility to attain the required filtering response [182]. But, a traditional half-mode cavity compromises on Q-factor due to the radiation from the open end. A novel design technique to model a second order SICL based bandpass filter with multiple transmission zeros in self-packaged form factor is conceived here. The proposed SICL cavity comprising of a L-bend line confined between a pair of dielectrics and shorted at both ends. A bandpass filter is devised by coupling a pair of half-mode cavities generated from the proposed SICL cavity. Further, in the designed bandpass filter selectivity is improved by placing a pair of transmission zeros on each lower and upper side of the passband. Later, three resonators are

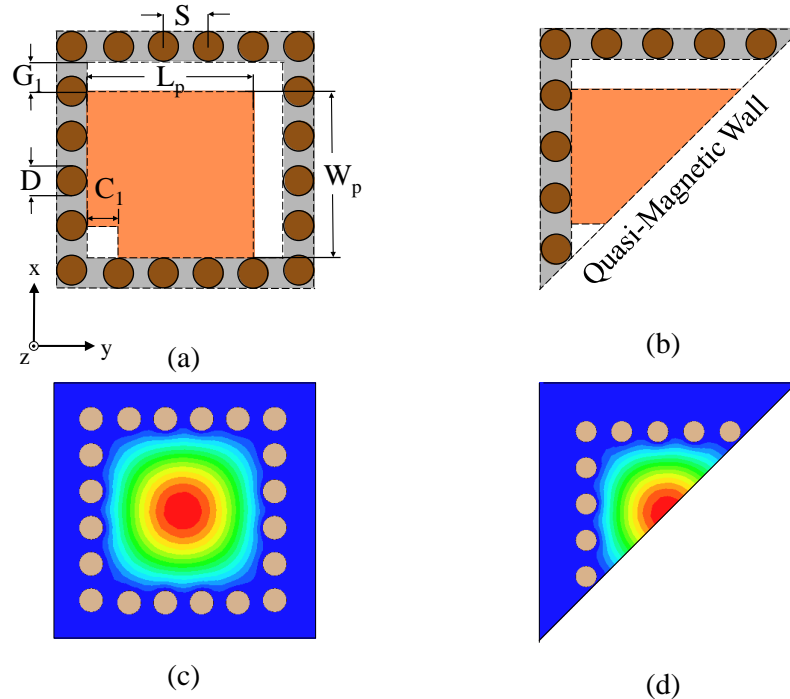


Figure 3.19 : Geometrical layout of proposed: (a) L-bend SICL cavity (b) Half-mode SICL cavity, Magnitude of E-field at first higher order mode in: (c) L-bend SICL cavity & (d) Half-mode SICL cavity.

embedded on the feed line to operate in out of band region of the bandpass filter to suppress the higher order modes and provide good out of the band performance with rejection level better than 20 dB, both below and above the passband.

3.3.1 Design of a compact SICL based cavity

The physical layout of the proposed substrate integrated coaxial line (SICL) cavity is shown in Fig. 3.19(a). A square patch (L_p) with a square-shaped corner cut (C_1) is confined between two layers of dielectric substrate which is bounded by rows of metallic vias shorting the adjacent sides of the patch. The other two sides are kept at G_1 distance from the via row. To enhance the coaxial nature of the designed cavity, a conducting strip with width same as the diameter of via is enforced through the vias. The entire configuration is enclosed by top and bottom conducting plates. The proposed design can essentially be treated as a L-bent SICL line with its first resonant mode occurring when L_p+W_p is around $\lambda_g/4$ at the resonant frequency. The half-mode variant of the proposed coaxial cavity is illustrated in Fig. 3.19(b). The electric field distribution of the fundamental TEM mode in proposed cavity is depicted in 3.19(c). A magnetic wall along the plane of symmetry is shown to preserve half field distribution of the cavity as depicted in Fig. 3.19(d). The proposed L-bent SICL cavity has side dimension L_p with spacing between the vias as S and diameter of via is D . In the above design, $S = 0.6\text{mm}$, $C_1 = 0.5\text{mm}$ and $D = 0.4\text{mm}$ to avoid any wave loss from the shielded cavity. In Fig. 3.20(a) and (b), the variation in resonant frequency of each mode as a function of L_p for the proposed cavity and its half-mode has been illustrated using the Eigen mode solver of Ansys High Frequency Structural Simulator (HFSS).

3.3.2 Modeling of a 2nd order SICL based bandpass filter with 4 transmission zeros: Filter A

The final layout of the proposed SICL bandpass filter is portrayed in Fig. 3.21 with dimensions and its construction is explained as follows. The half-mode of the proposed SICL cavity is fed by a $50\ \Omega$ SICL section. The magnitude of coupling can be modified by the depth (L_t) and gap of the inset (W_t). Excitation of higher order mode depends on the offset (Off_1) of $50\ \Omega$ feeding line from the center of the cavity. A second order bandpass filter is conceived by coupling the two half-mode cavities along their magnetic wall to form a completely shielded structure.

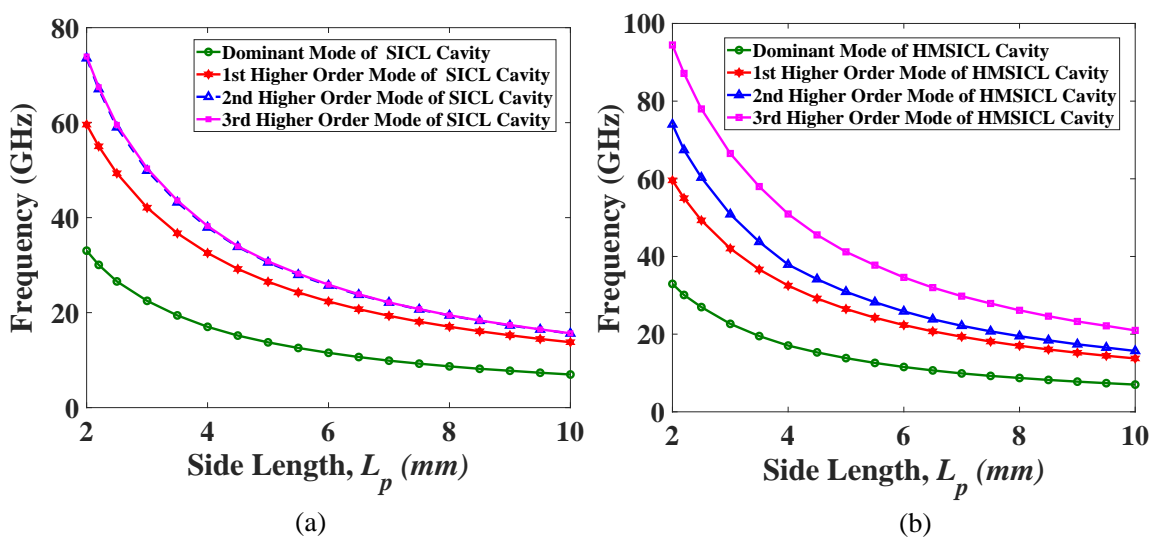


Figure 3.20 : Variation in resonant mode frequency as function of L_p in: (a) Proposed SICL cavity (b) Half-mode SICL (HMSICL) cavity.

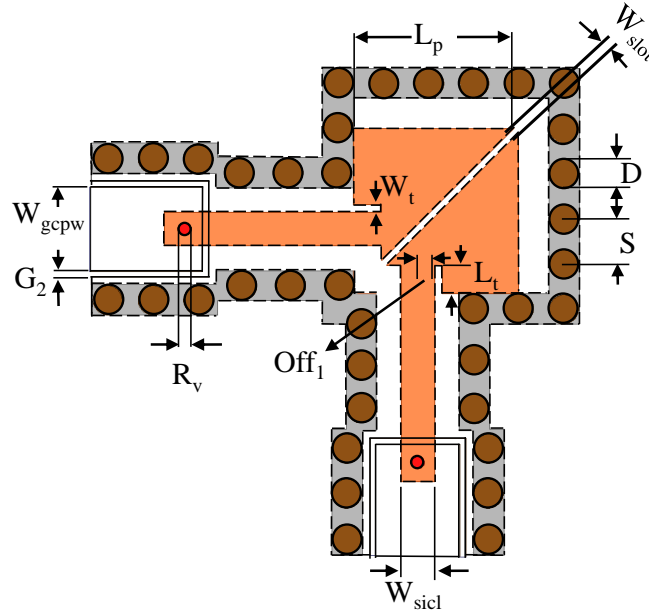


Figure 3.21 : Physical layout of the proposed *filter A* with dimensions: $G_1 = 0.4\text{mm}$, $G_2 = 0.1\text{mm}$, $D = 0.4\text{mm}$, $S = 0.6\text{mm}$, $R_v = 0.2\text{mm}$, $L_t = 0.34\text{mm}$, $L_p = W_p = 2.2\text{mm}$, $W_{gcpw} = 1.12\text{mm}$, $W_{sicl} = 0.44\text{mm}$, $W_{slot} = 0.13\text{mm}$ and $W_t = 0.15\text{mm}$

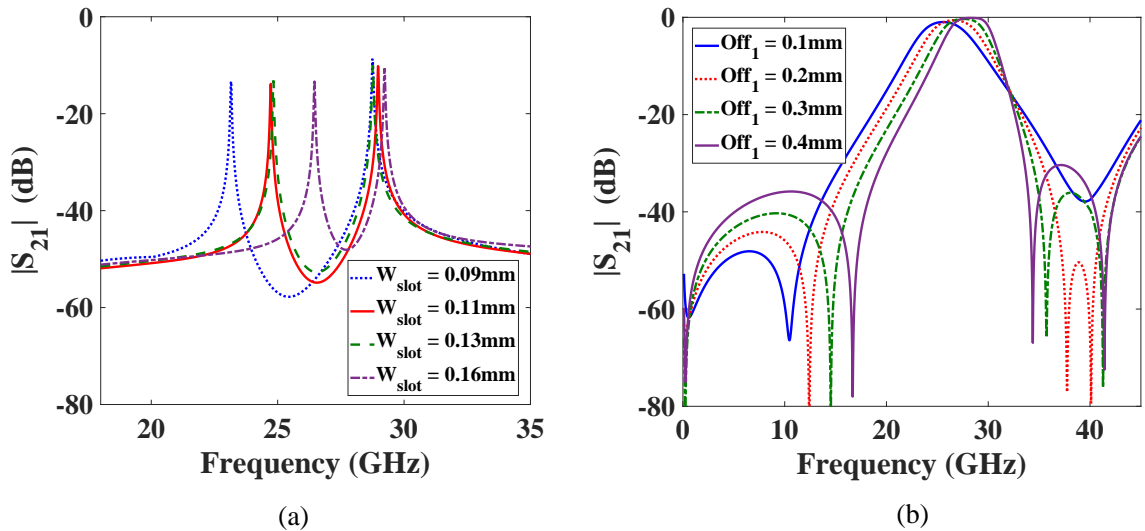


Figure 3.22 : Investigation on (a) dependence of self-resonance with W_{slot} under weak coupling (b) variation in $|S_{21}|$ with Off_1

The variation of self-resonance of the two half mode cavities as a function of gap (W_{slot}) between them under weak coupling has been studied in Fig. 3.22(a). The resonant mode less coupled to the source shifts towards the tightly coupled mode with increase in the coupling gap. Further, offset of feeding line from the center of cavity is investigated. Two transmission zeros are created on the upper side of passband at 33.92 GHz and 44.49 GHz due to the interaction between the pair of higher order orthogonal modes. These transmission zeros can be tuned by adjusting the coupling between higher order modes as seen from Fig. 3.22(b). The selectivity on the lower side of passband is improved by introducing transmission zeros at 0.36 GHz and 18.17 GHz by source

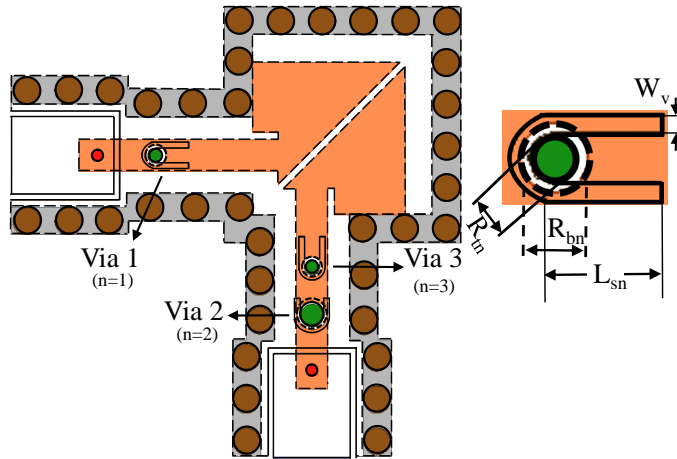


Figure 3.23 : Layout of the proposed *filter B* with dimensions: $L_{s1} = 0.6\text{mm}$, $L_{s2} = 0.57$, $L_{s3} = 0.38\text{mm}$, $R_{b1} = 0.2\text{mm}$, $R_{b2} = 0.18\text{mm}$, $R_{b3} = 0.32\text{mm}$, $R_{t1} = 0.22\text{mm}$, $R_{t2} = 0.2\text{mm}$, $R_{t3} = 0.34\text{mm}$, and $W_v = 0.1\text{mm}$

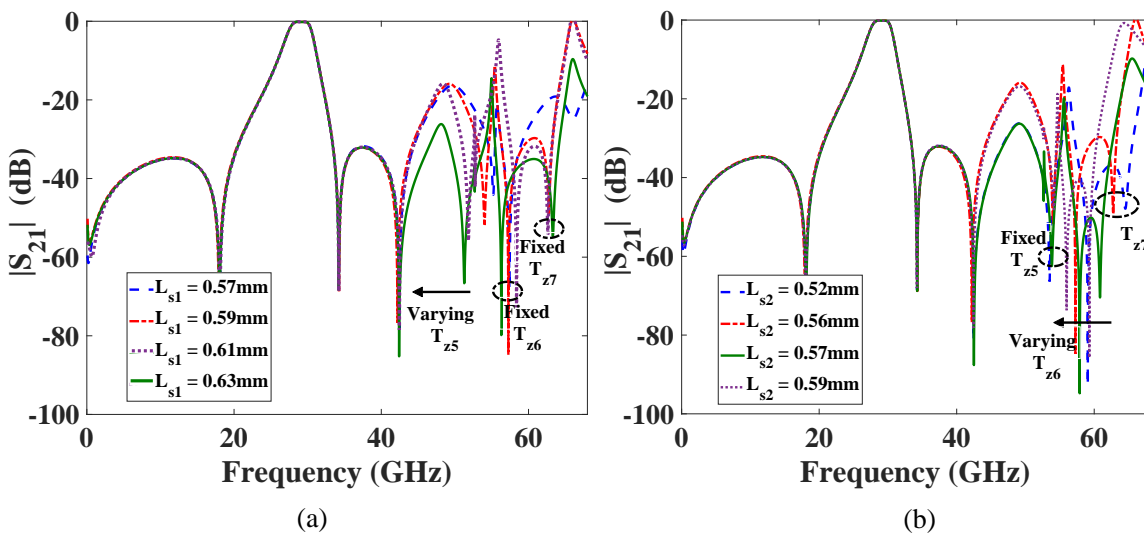


Figure 3.24 : Study of variation in location of (a) T_{z5} as a function of L_{s1} (b) T_{z6} as a function of L_{s2} .

to load coupling. The electromagnetically shielded second order filter exhibits low insertion loss in the passband. At least 20 dB out of the band rejection is achieved up to 45 GHz due to the transmission zeros created as seen in Fig. 3.22. A 3-dB passband from 26.6 GHz to 30.67 GHz i.e 14.21% fractional bandwidth is observed with a maximum insertion loss of 0.5 dB over 27.43 GHz to 29.92 GHz band.

3.3.3 Design of 2nd order SICL bandpass filter with enhanced out of band performance & higher order mode suppression: Filter B

A characteristic feature of bandpass filter is the ability to achieve wide out of the band rejection for enhanced performance of the system. Conventionally in waveguide based filters, band-reject response is produced by a partial height via post [68]. The location of the transmission

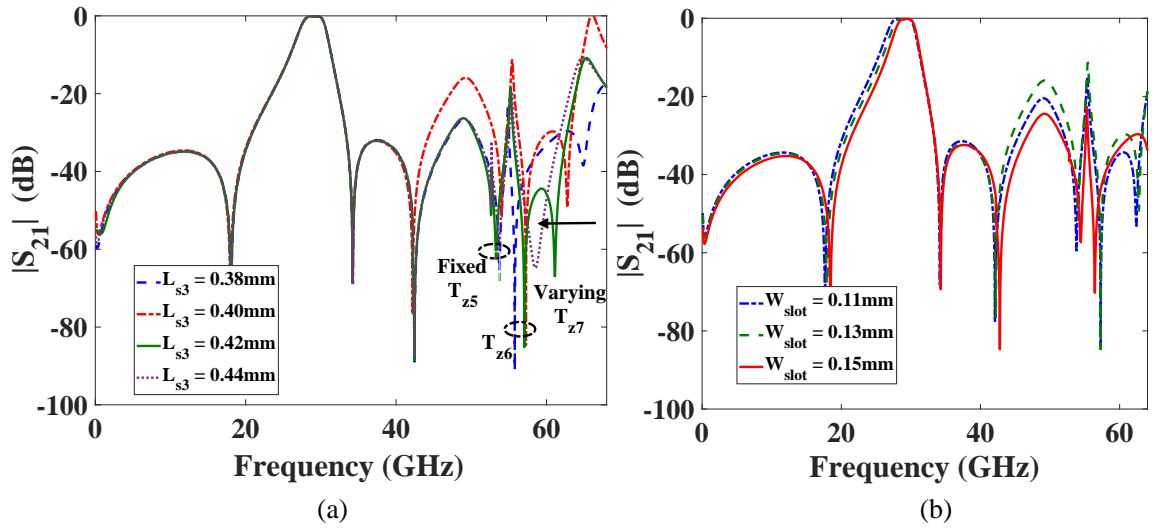


Figure 3.25 : Variation of (a) location of T_{z7} as a function of L_{s3} (b) W_{slot}

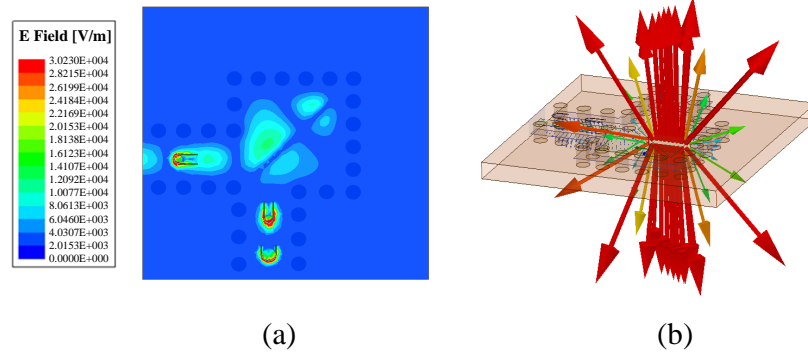


Figure 3.26 : Electric Field distribution in the proposed filter: (a) Magnitude of E-field at 62.67 GHz (T_{z7}) (b) E-field vector plot at 28 GHz.

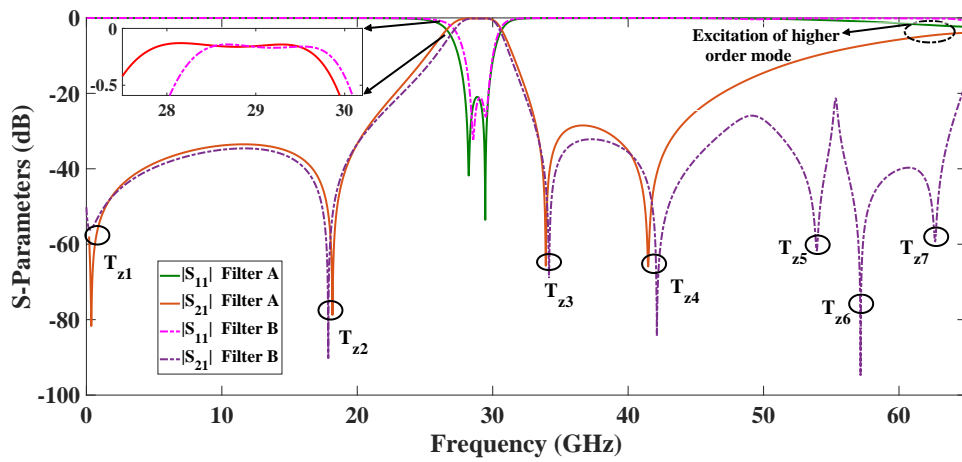


Figure 3.27 : Full-wave simulated S-Parameters of the designed second-order SICL based bandpass filters.

zero essentially depends on the gap between metal via post and top conducting plane of the waveguide, & its offset along the length of waveguide. The planar counterpart of this scheme is implemented in SIW technology using standard PCB technique by drilling metallic partial height vias in a thick substrate [70]. In these approaches, difficulty in achieving the required transmission zero lies in the intricate and complex fabrication process. In this work, the out of band response is improved by a bandstop filter topology comprising of metallic via from middle layer of a 50 Ω SICL section connecting the top conducting plate through a GCPW line as shown in Fig. 3.23. A slot of diameter R_b is cut in the central feeding strip to isolate the via from the SICL section. This configuration mimics the partial height via post by acting like a resonant element in the SICL section with a much simpler fabrication process. The geometrical layout of the proposed configuration is shown in Fig. 3.23. In Fig. 3.24 and Fig. 3.25 (a) the flexibility of additionally created transmission zeros is studied. By increasing the length of GCPW line (L_{s1}) connecting the via 1 ($n=1$) it is shown the fifth transmission (T_{z5}) shifts down in frequency with minimal change in position of sixth (T_{z6}) & seventh (T_{z7}) transmission zeros. From Fig. 3.25(b) we see varying L_{s2} varies the position of not just (T_{z6}) but also has effect on position of (T_{z7}). This is caused due to the closely placed bandstop resonators on the same feed line for achieving a compact size. A similar study is conducted in Fig. 3.25(a) for variation in L_{s3} . The dependence of out of band rejection in variation of W_{slot} is investigated in Fig. 3.25(b). It has been shown that by adjusting the length of the GCPW line (L_{sn}) the transmission zeros can be controlled and the out of band response can be extended. Three additional transmission zeros at 53.89 GHz, 57.16 GHz and 62.67 GHz are produced to suppress the first higher order mode. This kind of integration facilitates in extension of the out of band performance with minimal change in the original bandpass filter's response. A 3-dB passband from 27.17 GHz to 30.52 GHz i.e 11.21% fractional bandwidth is noted.

The proposed half-mode SICL bandpass filter is designed with a pair of low loss Rogers 5880 ($\epsilon_r = 2.2$, $\tan\delta = 0.0009$) substrate each of thickness 0.25 mm, which is bonded using Rogers 3001 prepreg ($\epsilon_r = 2.28$, $\tan\delta = 0.003$). A grounded-coplanar waveguide transition (GCPW) is realized by connecting a metallic via to the disconnected top layer from the SICL's middle layer. The performance of the proposed half-mode SICL filters are evaluated through the full-wave simulated scattering parameters generated by Ansys HFSS. The designed SICL bandpass *filter A* occupies 2.2 mm \times 2.2 mm or equivalently $0.3\lambda_g \times 0.3\lambda_g$ excluding the transition, where λ_g is guided wavelength at 28 GHz. Whereas, *filter B* with improved out of the band performance covers an area 6.47 mm \times 6.47 mm or equivalently $0.89\lambda_g \times 0.89\lambda_g$ including the feed line length and the transition, where λ_g is guided wavelength at 28 GHz. From the magnitude of E-field at the seventh transmission zero (T_{z7}) shown in Fig. 3.26(a) the extended out of band response contributed by the embedded via resonators can be perceived. Further, from Fig. 3.26(b), the radially outward electric field vector signifies the proposed SICL based filter to have electric field similar to that of traditional coaxial line in planar form. The full-wave simulated S-parameters of both the designed filters are as depicted in Fig. 3.27.

3.3.4 Results and Discussion

Due to the limitation in fabrication facility, as a proof of concept the proposed filter bandpass without any embedded resonators (filter A) is designed with center frequency at 10 GHz. The photograph of the fabricated prototype depicting the top and bottom view is shown in 3.28. The full-wave S-parameters obtained through Ansys HFSS are validated by experimental results recorded using Agilent E5071C network analyzer as shown in Fig. 3.29. A measured insertion loss of 1.69 dB is observed as compared to the simulated insertion loss of 0.46 dB as shown in the Fig. 3.29. The proposed bandpass filter exhibits a fractional bandwidth of 4.54% with 3-dB passband of 450 MHz centered at 9.91 GHz (f_o). The selectivity of the proposed SICL based filter is enhanced by transmission zeros produced on upper and lower edge of passband at 8.01 GHz and 11.05 GHz, respectively. A stop-band rejection level better than 30 dB up to 18 GHz is achieved in the proposed SICL based filter due to the additional transmission zero at 15.6 GHz. The slight

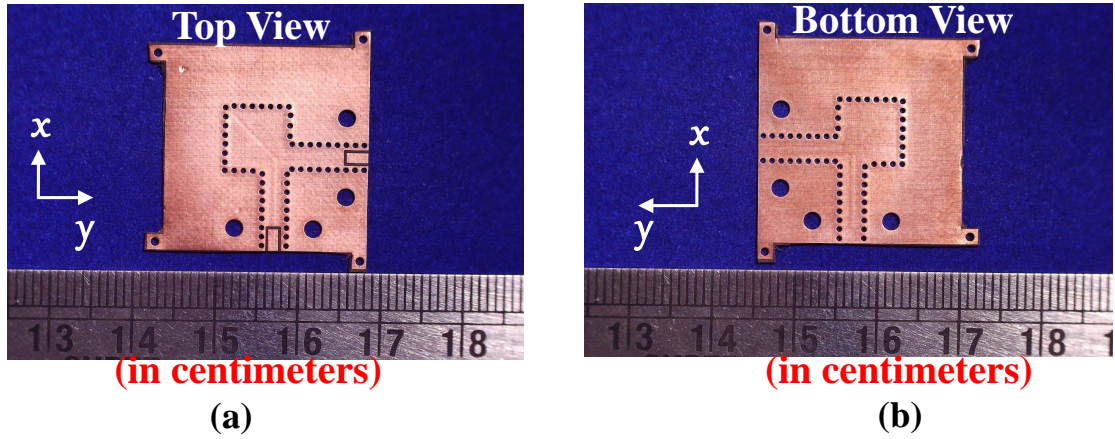


Figure 3.28 : Photograph of the proposed dual-mode SICL half-mode bandpass filter fabricated prototype operating at 10 GHz.

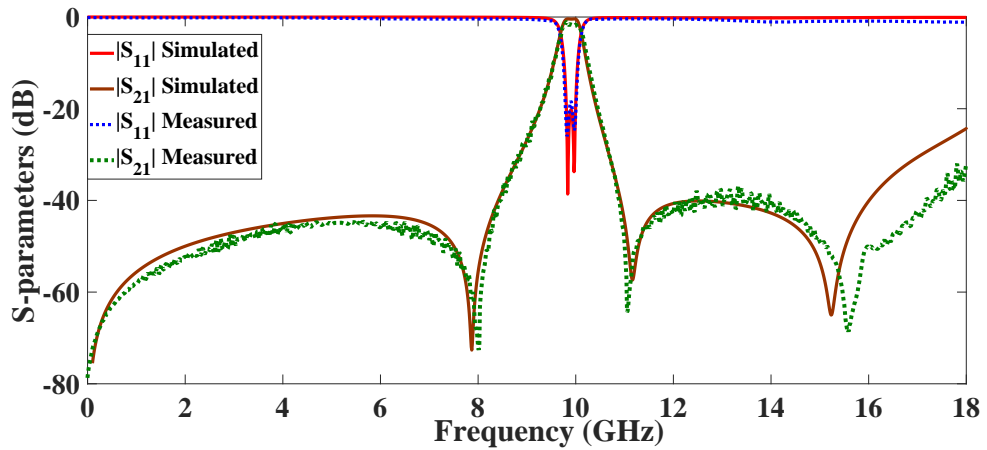


Figure 3.29 : Full-wave simulated and measured S-Parameters of the designed second-order SICL based bandpass filter (Proof of concept design at 10 GHz center frequency with dimensions: $G_1 = 0.4\text{mm}$, $G_2 = 0.2\text{mm}$, $D = 0.6\text{mm}$, $S = 1.1\text{mm}$, $R_v = 0.2\text{mm}$, $L_t = 0.69\text{mm}$, $L_p = W_p = 6.23\text{mm}$, $W_{gcpw} = 1.34\text{mm}$, $W_{sicl} = 0.48\text{mm}$, $W_{slot} = 0.24\text{mm}$ and $W_t = 0.25\text{mm}$).

discrepancy between simulated and measured results is attributed to fabrication tolerance and bonding of the multilayer PCB.

3.4 A SHIELDED COMPACT QUARTER-MODE SICL BASED DUAL-MODE DUAL-BAND FILTER FOR X AND K-BAND

The unprecedented growth of communication sector and the need for wide range of services for the consumers have created new requirements for RF design engineers/ scientists. One of the many challenges that currently needs to be addressed is the ability to operate at two individual frequencies in the millimeter-wave band with low loss in compact form factor. The following work discusses the design and development of a dual-mode substrate integrated coaxial line (SICL) based dual-bandpass filter with widely spaced passbands located in X and K-band. An SICL cavity conceived with L-shaped slots is investigated, and bisected along the fictitious

magnetic wall to derive its half-mode and quarter-mode counterparts. A fully shielded compact dual-mode dual-band filter is realized by coupling two quarter-mode cavities supporting TEM and TE_{110} mode of propagation in the lower and upper passband, respectively. The proposed SICL based filter realized using standard PCB fabrication process demonstrates ease of design and enhanced flexibility in exciting the higher order mode to attain the second-passband.

3.4.1 Geometry of the proposed SICL based cavity

The geometrical layout and layer-wise stack up of the proposed substrate integrated coaxial cavity is depicted in Fig. 3.30(a) and (b) respectively. The cavity developed in this work comprises of a short-circuited half-wavelength metallic strip sandwiched between two substrate layers each of thickness H . The entire structure bounded by four rows of copper plated vias along with top and bottom copper ground plate realizes the outer conductor of the planar coaxial cavity. In the middle layer, the low-impedance metallic strip is short circuited to diagonally opposite edges of the square cavity formed using plated through holes as shown in Fig. 3.30. The pitch between via holes and diameter of vias are chosen such that they preserve the shielded nature of the designed SICL cavity. In order to enhance the compactness of proposed structure, a stepped impedance line is realized in the middle layer instead of a low-impedance SICL line as shown in Fig. 3.31. Two L-shaped slots of side length S_l and width C_g are etched on diagonally opposite edges realize the non-uniform stepped-impedance line in middle-layer and preserve the shielded nature of the proposed cavity. Furthermore, the non-uniform stepped-impedance line in middle-layer aids in enhancement of miniaturization as observed from Table 3.2. The magnitude of electric field distribution in the proposed SICL cavity is shown in Table 3.3. The cavity is symmetrical along its diagonal plane symmetry AA' and BB . The radially outward vector electric field distribution asserts the presence

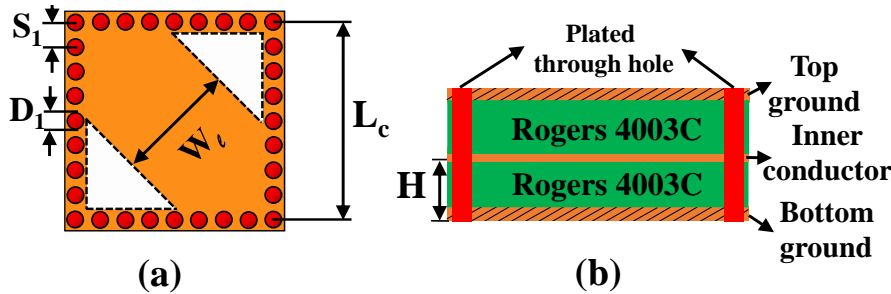


Figure 3.30 : Modeling of proposed substrate integrated coaxial line based cavity (a) physical layout with dimensions: $D_1 = 0.6\text{mm}$, $H = 0.8\text{mm}$, $L_c = 7.36\text{mm}$, $S_1 = 0.92\text{mm}$, $W_l = 4.51\text{mm}$ (b) stack-up of two-layer PCB.

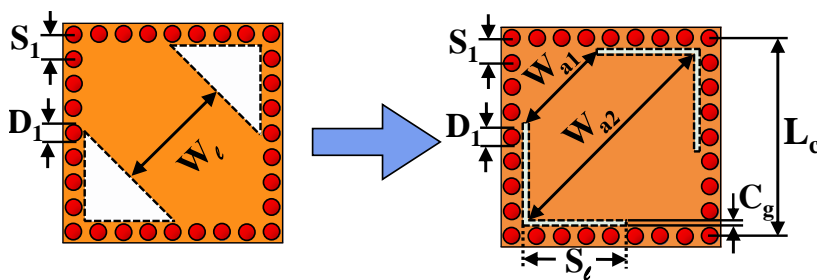


Figure 3.31 : Evolution of proposed substrate integrated coaxial line cavity with dimensions: $C_g = 0.2\text{mm}$, $S_l = 3.82\text{mm}$, $W_{a1} = 10.11\text{mm}$, $W_{a2} = 6.7\text{mm}$, $W_l = 6.7\text{mm}$

of coaxial like TEM based fundamental mode in the proposed planar cavity [90]. The lateral area of the cavity is reduced by 50% by creating a magnetic wall along the diagonal symmetry BB' and the half-field distribution of the cavity is preserved at same frequency as depicted by electric field in the half-mode SICL cavity in Table 3.3. On contrary to SIW half-mode, the open end of the central conductor is shielded in SICL half-mode cavity by the via wall of the outer conductor while maintaining PMC boundary along the symmetry plane which helps to reduce radiation loss and improves Q-factor. In order to further reduce the size of the cavity, a quarter-mode SICL based cavity is realized by bisecting the virtual magnetic wall of half-mode cavity formed along AA' . The variation in resonant frequency of each mode of the proposed SICL based cavity, its half-mode and quarter-mode variant as a function of its side length (L_c) is recorded in Fig. 3.32(a) using the Eigen mode solver of Ansys HFSS. The magnitude of electric field distribution of first higher order mode of SICL cavity, its half-mode and quarter-mode variant are shown in Table 3.2. The SICL cavity and its half mode variant support TEM_2 mode as its first higher order mode. But the quarter-mode

Table 3.2 : Study on frequency of fundamental mode in proposed SICL cavity

Topology	Shorted $\lambda_g/2$ SICL Line	Proposed SICL Cavity
Fundamental mode	10.247 GHz	9.641 GHz

Table 3.3 : Electric field distribution of resonant modes shown in the top ground plane of proposed SICL cavity

	Layout	Fundamental mode	1 st higher order mode
SICL cavity			
Half-mode cavity			
Quarter-mode cavity			

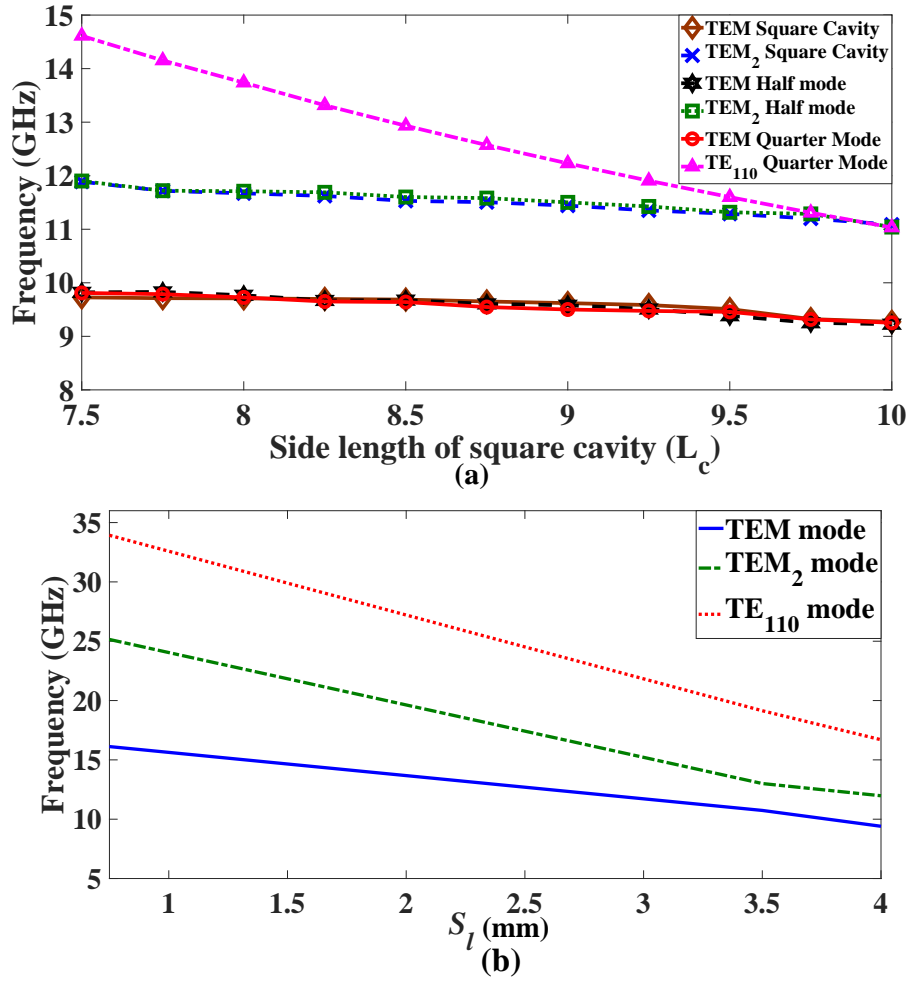


Figure 3.32 : Mode chart depicting variation in resonant frequency as a function of (a) side length (L_c) (b) slot length (S_l)

cavity due to the open boundary condition exhibits TE_{110} as next higher order mode. The L-shaped slots in the middle layer of the proposed SICL cavity provides another degree of freedom to control the resonant frequency of fundamental and higher order modes as observed in Fig. 3.32(b). The proposed SICL cavity demonstrates a 59.8% size reduction as compared to its SIW counterpart.

3.4.2 Design of a single-band dual-mode SICL bandpass filter

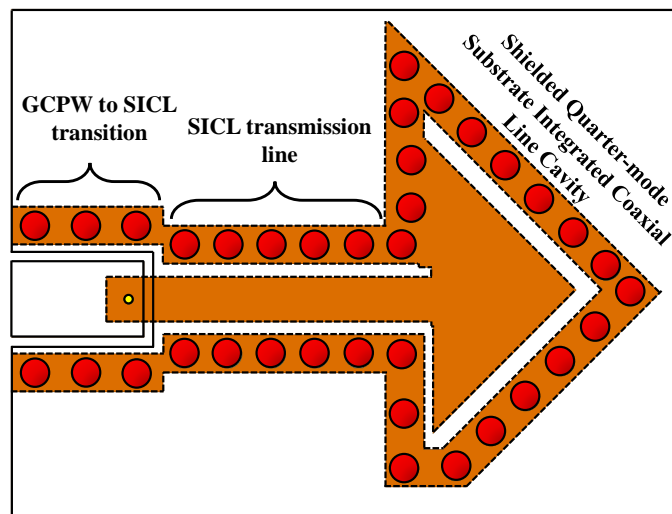
In order to utilize the proposed cavity as a bandpass filter it needs to be excited using an external circuitry. The feeding mechanism of the shielded quarter-mode cavity is shown in Fig. 3.33(a). An SICL transmission line is fed with certain offset from the center to the proposed shielded quarter-mode cavity. Further, the SICL line is inset into the cavity controls the strength of coupling. In SICL technology there is a need for transition as the inner conductor is not exposed for testing. SICL to GCPW transition is realized using a plated blind via connecting the SICL line with the GCPW line. The electric field distribution in the proposed single port cavity is depicted in Fig. 3.33(b). One of the prominent features of the proposed shielded quarter-mode cavity is that the electric field distribution is limited with the via walls to provide excellent electromagnetic compatibility and finds application in densely integrated RF front-end. The reflection coefficient of the singly loaded cavity is shown in Fig. 3.34. To understand the characteristics of the proposed quarter-mode cavity, its external quality factor is computed in Fig. 3.35. The procedure to compute

the external quality factor is discussed in Fig. 3.35(a), where the phase and group delay of proposed cavity are recorded using a full-wave simulator such as Ansys HFSS. The external quality factor is computed as (3.1) and is shown for the proposed cavity in Fig. 3.35(b).

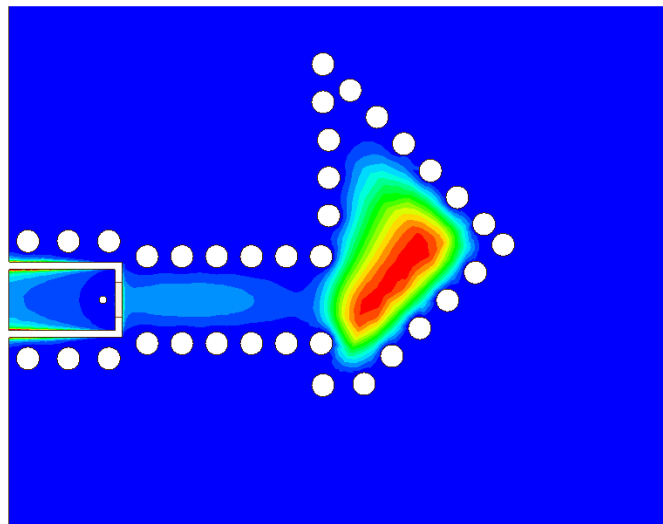
$$Q_{ext} = \frac{f_o}{\Delta f} \quad (3.1)$$

Where the fractional bandwidth (Δf) is chosen as difference between the frequencies where the phase is $\pm 90^\circ$ with respect to the phase at group delay peak. The group delay peak is considered to determine resonant frequency as the resonant frequency determined from S-parameters may differ due to loading effect [80].

The physical layout of the proposed dual-mode SICL based BPF is depicted in Fig. 3.36. In this work, two quarter-mode SICL cavities are coupled along their magnetic wall similar to the previously discussed inter-coupled half-mode mode cavities in section 3.2 to realize a second-order



(a)



(b)

Figure 3.33 : Feeding mechanism of the proposed fully shielded quarter-mode SICL cavity (a) Layout (b) Electric field distribution at fundamental mode

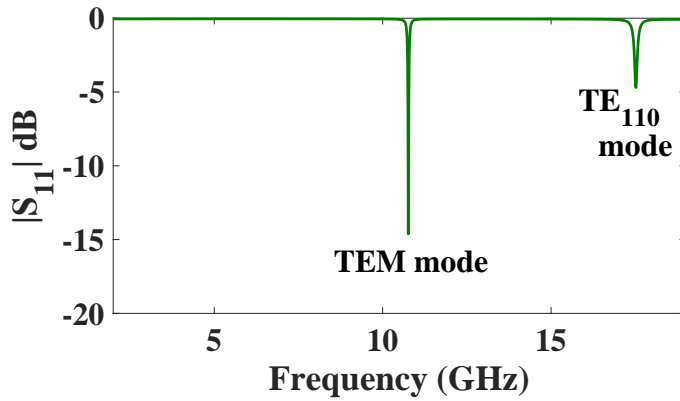


Figure 3.34 : Full-wave simulated reflection coefficient of the shielded quarter-mode SICL cavity

bandpass filter. A plated via row is placed at a distance G_1 from the other magnetic wall of the two cavities to form a completely shielded structure. The 50Ω SICL feeding lines are arranged orthogonal to each other. The inset of feed line (In) controls the coupling to the quarter-mode

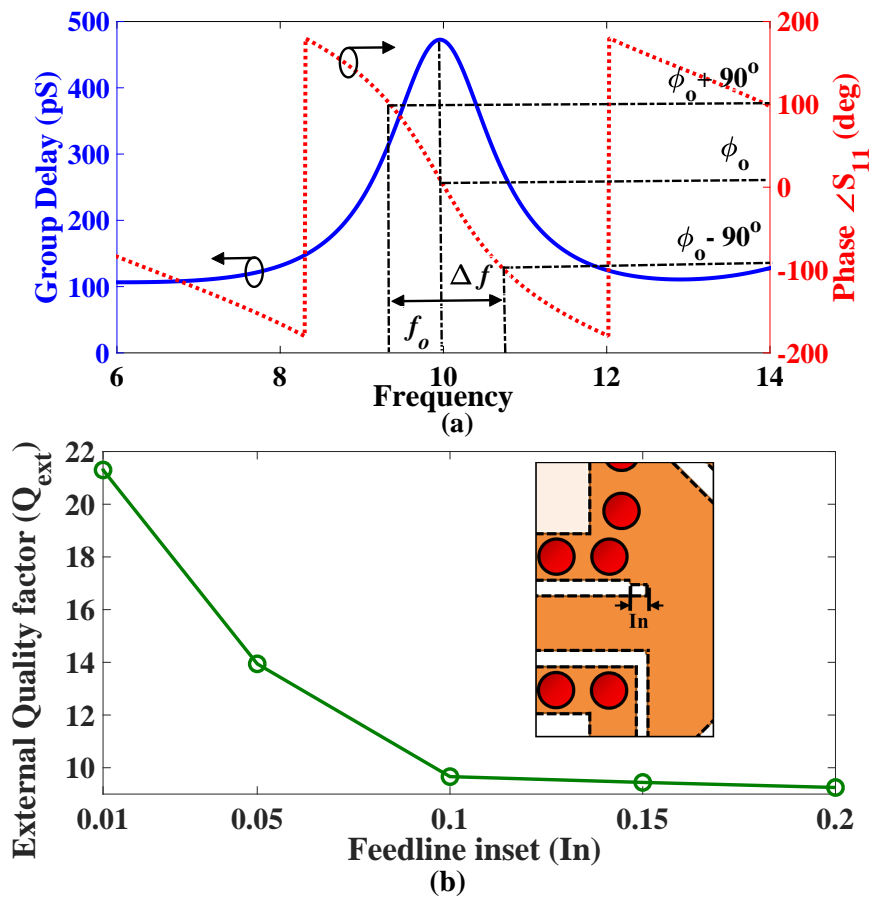


Figure 3.35 : Calculation of external quality factor of SICL based shielded quarter-mode cavity (a) Phase response and group delay (b) Variation of external quality factor with change in feedline inset (In)

cavity and is adjusted appropriately for good impedance matching. Further, the feedline is offset from center of cavity by 1.5mm to only excite the fundamental mode of the quarter-mode SICL cavity. A single band-filter with transmission zeros is designed using the fundamental TEM mode of the two inter-coupled quarter-mode SICL cavities. The coupling coefficient between the two inter-coupled quarter-mode SICL cavities is computed by varying S_g as shown in Fig. 3.37 (a). The proposed filter exhibits a fractional bandwidth (FBW) of 8.8%, or equivalently 3-dB passband of 1107 MHz centered at 12.59 GHz with transmission zeros on lower and upper side of the passband. The elements of coupling matrix for the proposed bandpass filter is computed using (3.2) for center frequency f_o , fractional bandwidth FBW , and external quality factor Q_e [80]:

$$M_{Si} = \frac{1}{\sqrt{FBW}Q_{ei}}, Q_{ei} = \frac{\omega_i G D_{S_{11}}(f_i)}{2} \quad (3.2a)$$

$$M_{Li} = \frac{1}{\sqrt{FBW}Q_{ei}}, Q_{ei} = \frac{\omega_i G D_{S_{22}}(f_i)}{2}, i = 1, 2, \dots, N \quad (3.2b)$$

$$M_{ii} = \frac{f_o^2 - f_i^2}{BW \times f_i} \quad (3.2c)$$

The synthesized coupling matrix of the proposed single-band filter is given in (3.3).

$$M = \begin{bmatrix} S & 1 & 2 & L \\ S & 0 & 1.2179 & 0 & -0.0215 \\ 1 & 1.2179 & 0.2988 & 1.6161 & 0.2375 \\ 2 & 0 & 1.6161 & -0.3443 & 1.1932 \\ L & -0.0215 & 0.2375 & 1.1932 & 0 \end{bmatrix} \quad (3.3)$$

The comparison between the synthesized filter and full -wave simulated SICL based bandpass filter is shown in Fig. 3.37 (b). The calculated second-order coupling matrix takes the two fundamental modes of the inter-coupler quarter mode cavities in to consideration to generate the S-parameters of synthesized filter.

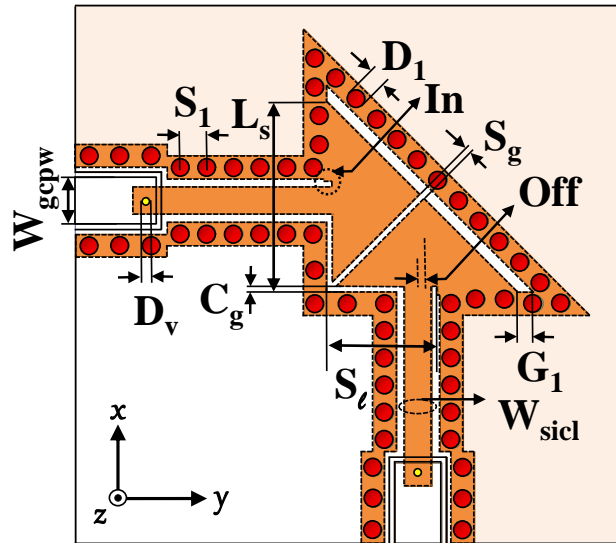


Figure 3.36 : Proposed SICL based dual-mode single/dual-band filter layout with dimensions: $C_g = 0.2\text{mm}$, $D_v = 0.6\text{mm}$, $G_1 = 1\text{mm}$, $In = 0.28\text{mm}$, $L_s = 6.58\text{mm}$, $S_1 = 0.95\text{mm}$, $S_g = 0.19\text{mm}$, $S_l = 3.82\text{mm}$, $W_{cpw} = 1.6\text{mm}$, $W_{sicl} = 0.94\text{mm}$, $Off = 1.5\text{mm}$ (single-band), 0.3mm (dual-band)

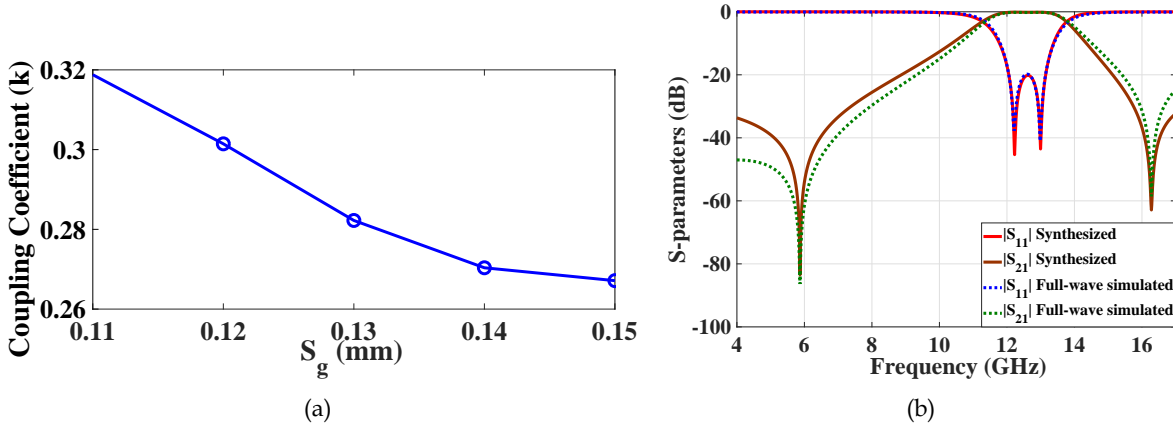


Figure 3.37 : Study of the proposed SICL based quarter-mode filter (a) Calculation of coupling coefficient with variation in S_g (b) Comparison between filter response generated using coupling matrix and the full-wave simulated S-parameters

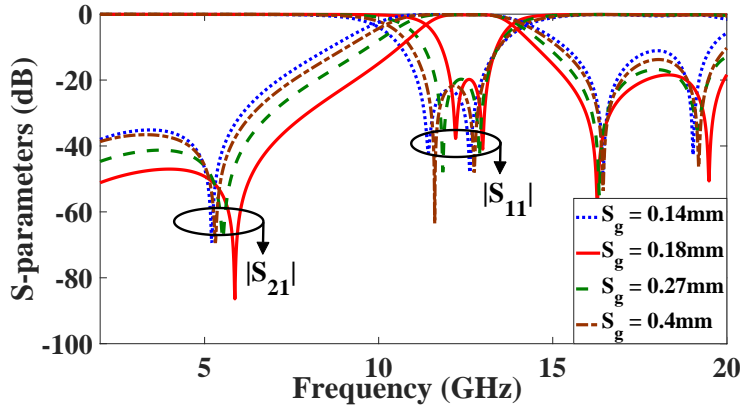


Figure 3.38 : Flexibility in adjusting the bandwidth of proposed single-band SICL based BPF.

3.4.3 Development of a dual-mode dual-band SICL based BPF

The dual-band operation in the proposed SICL based bandpass filter can be achieved by modifying the offset as shown in Fig. 3.36. The lower band and higher band of the proposed dual-band filter is realized using the SICL quarter-mode cavity which supports TEM mode and TE_{110} mode of propagation, respectively as shown in Table 3.3. The coupling between the two quarter-mode SICL cavities to obtain the desired dual-band operation is controlled through gap (S_g) and offset of feed line (Off). The feed line is offset from center of cavity by 0.3mm to excite the fundamental (TEM) and first higher order mode (TE_{110}). The upper passband centered at 19.21 GHz is guarded by two transmission zeros created due to the interaction between the higher order orthogonal modes and source to load coupling, respectively. Change in width of the L-shaped slot etched in the middle layer of SICL cavity perturbs the higher order mode & aids in independently tuning the center frequency of band II as shown in Fig. 3.40(a). Further, weak source to load cross-coupling introduces a transmission zero on the lower side of band I [183]. In Fig. 3.40(b), parametric analysis shows as the feed lines are offset from each other the transmission zeros produced by source to load coupling disappear [184]. The aforementioned studies suggest the following design steps:

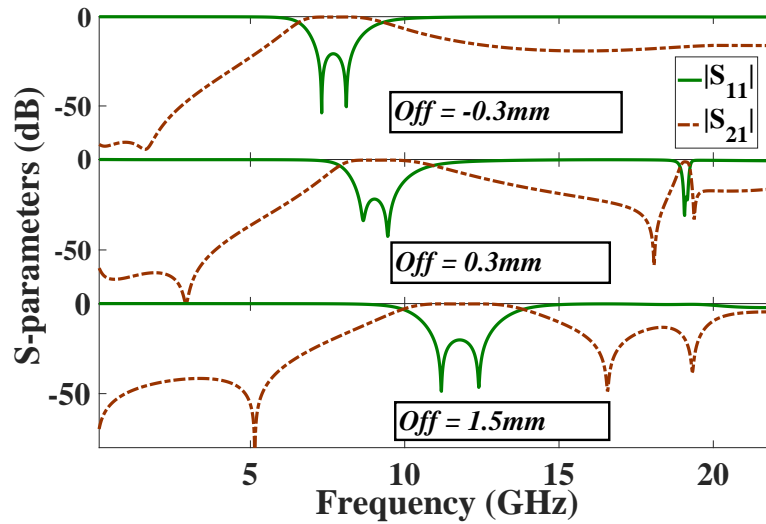


Figure 3.39 : Flexible response in proposed BPF with change in feedline position

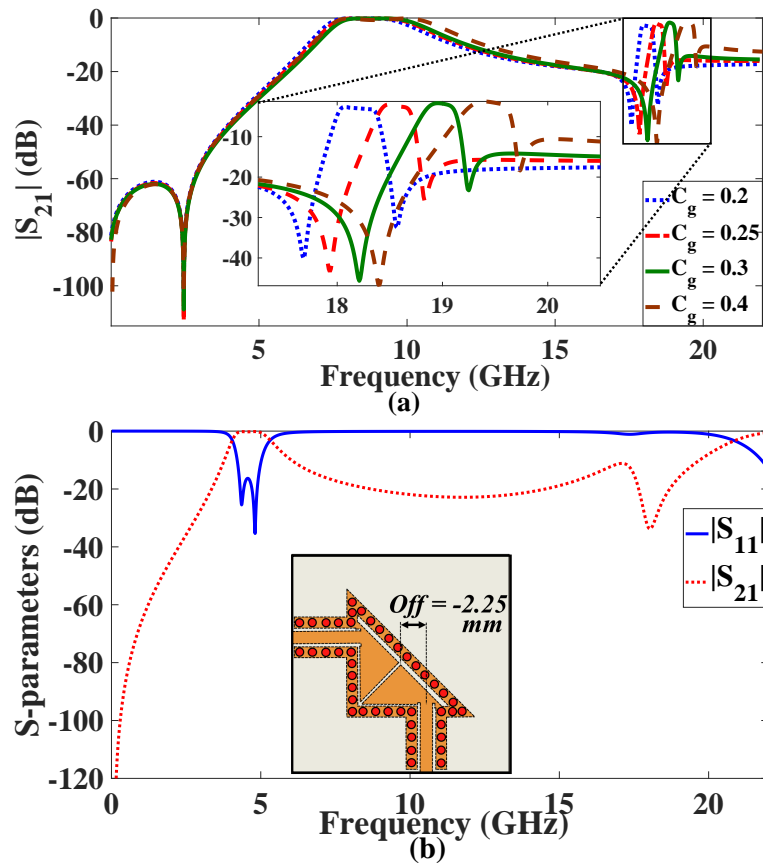


Figure 3.40 : Investigation on (a) change in slot width (C_g) for independently tuning band II (b) effect on source-load coupling due to offset of feedline (Off)

1. Using the mode chart in Fig. 3.32 select the dimension (L_s) of proposed filter to operate at the desired frequency. The fundamental mode occurs approximately at a side length $\lambda_g/2$. The slot

length S_l provides another degree of freedom to tune the frequency of operation.

2. Decide whether single or dual-band operation is required. Offset the feedline less than $\lambda_g/20$ approximately from the center of cavity to excite the higher order mode and achieve dual-band operation.
3. To tune the upper-passband of dual-band filter, optimize the slot width C_g or add a perturbation to disturb the higher order mode.
4. Optimize inset (In) width and length for the best impedance matching characteristics.

3.4.4 Design flexibility of proposed SICL based BPF

The bandwidth of single-band filter can be flexibly tuned by varying the coupling gap (S_g) between the two cavities. Using a full-wave simulator such as Ansys HFSS it is shown that the maximum achievable fractional bandwidth using this technique is 38.8% and the fractional bandwidth can adjusted anywhere between 8.8% and 38.8% as shown in Fig. 3.38 by suitably choosing the coupling gap between the inter-coupled quarter-mode cavities. Further, the proposed SICL based filter provides flexible response by the virtue of simple design topology. Single band and dual-band operation with multiple transmission zeros can be realized by exciting the cavity with appropriate offset of feedline as shown in Fig. 3.39. The center frequency of the upper-passband of dual-band filter can be independently controlled by adjusting the slot width C_g .

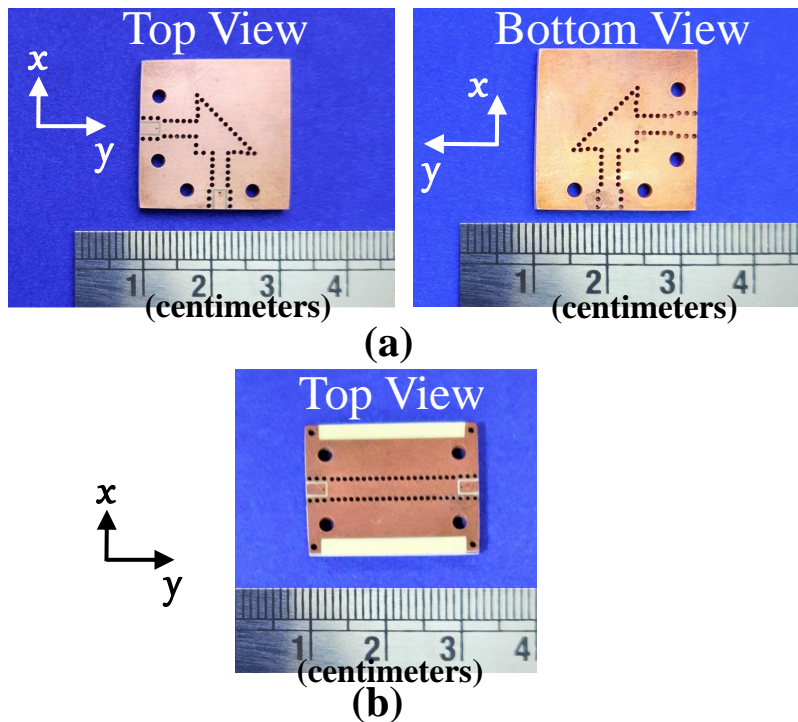


Figure 3.41 : Photograph of (a) the fabricated SICL-based dual-band filter (b) Back to back GCPW to SICL transition fabricated on Rogers 4003C substrate with 1.6mm thickness.

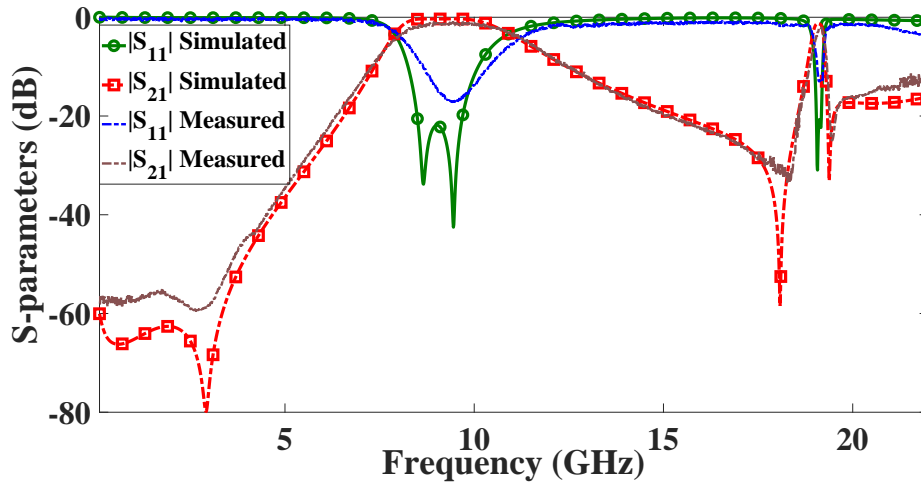


Figure 3.42 : Comparison between full-wave simulated and measured results of the proposed SICL based dual-mode dual-band bandpass filter

3.4.5 Results & Discussion

To experimentally validate the quarter-mode SICL cavity, a dual-bandpass filter based on inter-coupled quarter-mode SICL cavity is fabricated using a pair of Rogers 4003C ($\epsilon_r = 3.38$, $\tan\delta = 0.0027$) substrates each of thickness 0.8 mm. Photograph of the fabricated prototype depicting the top and bottom view is shown in Fig. 3.41 (a). The full-wave simulated filter response generated using Ansys HFSS is confirmed by measuring the scattering parameters of proposed filter prototype using Agilent N5234A vector network analyzer as shown in Fig. 3.42. The proposed widely spaced passbands of SICL bandpass filter demonstrate a 3-dB bandwidth of 3.18 GHz and 0.27 GHz centered at 9.61 GHz and 19.12 GHz, respectively. The deviation in measured filter response maybe attributed to fabrication tolerance and minor air-gaps between the stacked dielectric substrates. Further, the measured insertion loss at the two passband is recorded as 1.34 dB and 2.08 dB as compared to the simulated insertion loss of 0.4 dB and 1.26 dB, respectively. The measured insertion loss takes in to account the two SICL-GCPW transitions to accommodate K-type connectors. To study the effect of GCPW transition on the performance of proposed BPF, an SICL transmission line of length 24mm with back to back GCPW transition is fabricated on Rogers 4003C substrate with 1.6mm thickness as shown in Fig. 3.41(b). A comparative study of SICL line with and without transitions indicates a measured insertion loss of 2 dB with return loss better than 10 dB at 20 GHz in Fig. 3.43. It is to be noted the GCPW transitions are required only to test the component individually and losses due to them would not be accounted when used in a system. The parasitics due to blind via in an SICL-GCPW transition can be reduced by using a low-profile/smaller thickness substrate [91] for better insertion loss of designed filter. In order to compare the performance of the proposed SICL based filter with previously reported bandpass filters, Table III is considered. Microstrip technology is preferable for design of filters for below 10 GHz and the literature provides several single/dual bandpass filters for the same. However, these design techniques when scaled to operate in X-band and above demonstrate significant insertion loss [185, 21] due to radiation loss and surface-wave loss. Widely used SIW technology as an planar alternative to waveguide to design shielded filters suffer from large size, have narrow-monomode bandwidth and cannot support dual-band filters with large frequency ratio as seen from Table 3.4.

The notable features of proposed dual-band SICL bandpass filter are discussed in brief as below:

Table 3.4 : Comparison of proposed work with state of art bandpass filters

Ref	Tech.	f_1/f_2	FBW	$ S_{21} $ (dB)	Size (λ_g^2)	Δ $= (f_2/f_1)$
[74]	LTCC	14.52/-	7.57	3.27/-	0.37	-
[185]	Microstrip	10/-	13.2	2.07/-	N.M	-
[21]	Microstrip	13.31/-	4.7	2.1/-	0.12	-
[186]	SIW	9.5/10.5	2.4/1.8	1.28/1.55	0.76	1.1
		12/14	5.53/ 4.04	1.21/1.34	2.77	1.16
[85]	SIW	12/16	3.8/ 3.47	1.79/1.76	2.7	1.33
		12/17	5.08/ 2.72	1.39/2.47	2.9	1.41
		12/16	8.75/7.06	1.07/1.95	1.92	1.33
[86]	SIW	12/15	7/6.6	1.24/0.85	2.14	1.25
		12/17	6.87/3.26	1.16/2.32	1.16	1.41
[87]	CSIW	9.94/13.9	4.3/4.2	2.89/3.53	N.M	1.39
[187]	SIW	17.24/20.17	1.4/2.08	1.8/1.9	1.64	1.17
[88]	HMSIW	5/7.5	5.46/4.75	1.65/2.25	1.53	1.5
		5/8.5	6.26/7.75	2.02/1.82	1.1	1.7
[188]	SIW	4.6/5.3	2/1.5	1.95/2.75	1.37	1.15
TW	SICL	9.61/19.12	33.1/1.41	1.34/2.08	0.15	1.99

TW: This work, N.M: Not mentioned, Δ : Frequency ratio (f_2/f_1)

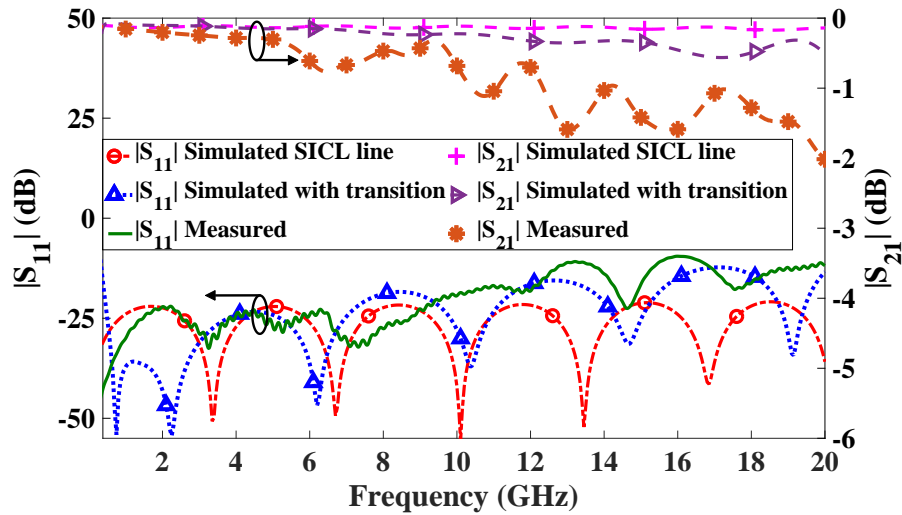


Figure 3.43 : Performance of SICL transmission line with and without GCPW transitions designed & fabricated on 1.6mm thick Rogers 4003C substrate

1. The proposed dual-mode dual-band filter is completely shielded by the outer conductor formed by lateral vias and ground planes. With no slots etched on the top/bottom ground planes the

proposed filter provides excellent electromagnetic robustness.

2. Design of a dual-mode dual-band BPF in SICL technology facilitates widely separated passbands in X and K band respectively with a frequency ratio of 1.99, which is higher than the recently reported dual-band BPF [186, 85, 86, 87, 88, 187, 188].
3. The proposed topology provides flexible filter response for single/dual-band operation with multiple transmission zeros by controlling the position of feedline (*Off*). Further, the bandwidth of single-band filter can be flexibly controlled just by varying the coupling gap (S_g) between the two cavities achieve a fractional bandwidth between 8.8% to 38.8%.
4. Utilization of compact inter-coupled quarter-mode SICL cavity for the proposed dual-band filter design takes up only 45.32 mm^2 lateral area, equivalently $0.15 \lambda_g^2$, where λ_g is the guided wavelength at 9.61 GHz. Further, the proposed SICL cavity demonstrates a 59.8% size reduction as compared to its SIW counterpart.
5. The TEM mode of operation provides enhanced bandwidth (33.1% FBW) in SICL cavity filters as compared to other $X/K_u/K$ [186, 85, 86, 87, 88, 187, 188] filters.

3.5 TRIPLE-MODE SUBSTRATE INTEGRATED COAXIAL RESONATOR BASED BANDPASS FILTER FEATURING FLEXIBLE TRANSMISSION ZEROS AND ADJUSTABLE BANDWIDTH

The popularly synthesized substrate integrated coaxial line (SICL) based components though provide good design flexibility, they ultimately increase the fabrication complexity and thereby the overall cost. In the following work substrate integrated coaxial resonator (SICR) based triple-mode bandpass filters designed for K_u -band on a single-layered dielectric substrate. A self-shielded SICR based third-order filter is realized using two planar coaxial resonators (SICR) embedded in a substrate integrated waveguide cavity (SIW). Merging the TEM based mode of two SICR's with TE_{101} mode of SIW significantly enhances the bandwidth in a compact size. A novel topology realized using short circuited metallic via connecting to the top conducting plane through a metal strip demonstrates high degree of flexibility in positioning the transmission zeros to improve the selectivity as well as extend the out-of-band rejection of proposed filter. Finally, three experimental prototypes are fabricated and tested for K_u -band to affirm the wide-bandwidth, enhanced selectivity and good out of band rejection of the proposed filter synthesis methodology.

3.5.1 Modeling of triple-mode SICR bandpass filter: Filter C

The modeling of proposed triple-mode filter starts with design of an SIW cavity. The square-shaped SIW cavity of side length W_s is realized by series of four metallic via rows connecting the top and bottom copper layers that are separated by a single layer of dielectric substrate. The S-parameters of the SIW cavity without any loading elements has been shown in Fig. 3.44(a). As expected a narrowband bandpass response with resonant frequency at 17.85 GHz is noted. In Fig. 3.44(b) the electric field distribution in cavity shows a dominant TE_{101} mode in the cavity without any loading elements. The proposed filter has a slot of width W_{g1} is etched along the vertical plane of symmetry to form a half-mode cavity with length L_{hm} and width W_s . The proposed topology comprises of a copper plated via connected to a circular disc that is capacitively coupled to the top ground plane of the cavity and directly connected to bottom ground plane. The copper plated via with diameter D_{x1} and rows of via forming the square cavity make the inner and outer conductor of this substrate integrated coaxial resonator (SICR), respectively. Similarly another SICR with inner conductor of diameter D_{x2} is embedded as shown in Fig. 3.45. The two SICR are offset by a distance px_1 and px_2 from the center respectively to adjust the coupling between the modes. A transmission zero on the upper side of passband is produced due to transversal signal interaction

of the two paths created between input and output by each SICR. This is verified from Fig. 3.46 where the position of SICR's are offset from center to vary path length between input and output to control the position of transmission zero. Further, self-resonant frequency of each mode of the proposed filter is analyzed by applying a weak input to the as shown in Table 3.6(a)-(c). The 3rd self-resonant frequency is contributed by the TEM mode of SICR can be tuned independently by varying D_{c1} as shown in Table 3.6(a) and the same is affirmed by the concentration of E-field around the upper SICR. The second-self resonant frequency is contributed by half-mode SIW and can be controlled by varying the width of cavity (L_{hm}) as verified from S-parameters and electric field distribution in Table 3.6(b). Due to strong coupling between the two SICR's as shown Table 3.6(c) it is observed that by changing the diameter D_{c2} of circular patch, first as well as third self resonant frequency vary. Further, the characteristic impedance of the TEM based SICR can be varied by

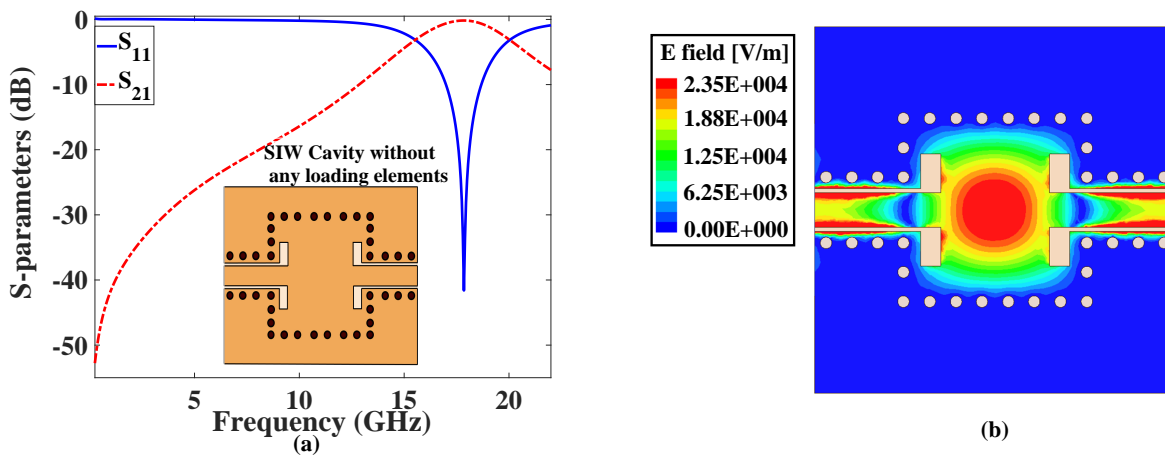


Figure 3.44 : SIW cavity without any loading elements (a) S-parameters (b) E-field distribution in dominant mode

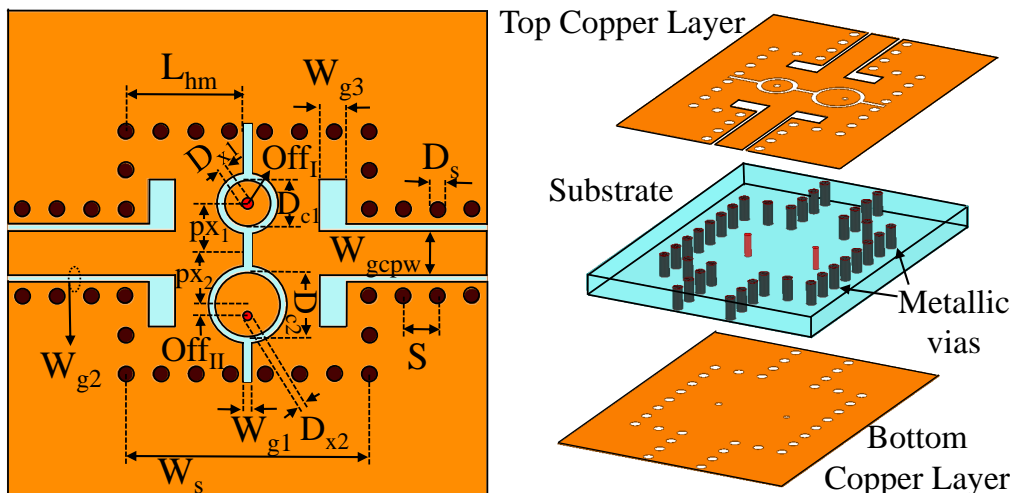


Figure 3.45 : Geometrical layout of triple-mode SICR based bandpass filter (Filter C) with dimensions: $D_{C1} = 1.2\text{mm}$, $D_{C2} = 1.7\text{mm}$, $D_s = 0.4\text{mm}$, $D_{x1} = 0.28\text{mm}$, $D_{x2} = 0.24\text{mm}$, $L_{hm} = 3.09\text{mm}$, $Off_I = 0\text{mm}$, $Off_{II} = 0.3\text{mm}$, $px_1 = 1.3\text{mm}$, $px_2 = 1.35\text{mm}$, $S = 0.9\text{mm}$, $W_{gcpw} = 1.2\text{mm}$, $W_{g1} = 0.21\text{mm}$, $W_{g2} = 0.15\text{mm}$, $W_{g3} = 0.7\text{mm}$, $W_s = 6.4\text{mm}$.

adjusting the position (Off_1) and diameter of inner conductor (D_{x1}, D_{x2}) to obtain good impedance matching as shown in Fig. 3.47. Coupling matrix theory is used to develop a lumped model[80] and analyze the electromagnetic coupling between the LC resonators representing the three modes of proposed filter. Fig. 3.48 illustrates the lumped model of triple-mode filter and the synthesized coupling matrix developed using the procedure described in [80]. The synthesized filter response is compared with full-wave and measured results in section 3.5.5.

3.5.2 Design of SICR bandpass filter with flexible transmission zero: Filter D

In this work a planar counterpart of a partial height [102] via is proposed to integrate with bandpass filter to produce a flexible transmission zero. The geometrical layout of the proposed filter (Filter D) is shown in Fig. 3.49. On the GCPW feed line of filter C, a metallic via is connected to a circular patch that is isolated from the bottom ground plane. Further, the via is connected to the signal line of GCPW through a metallic strip of length L_{sn} (where $n = 1$) as shown in inset of Fig. 3.49. The above proposed topology can be decomposed into three parts, i) Metallic via coupled to signal line of GCPW line ii) metallic via connected to signal line of GCPW through a metal strip and iii) a transmission line to which the metal strip is connected. The metallic via capacitively coupled

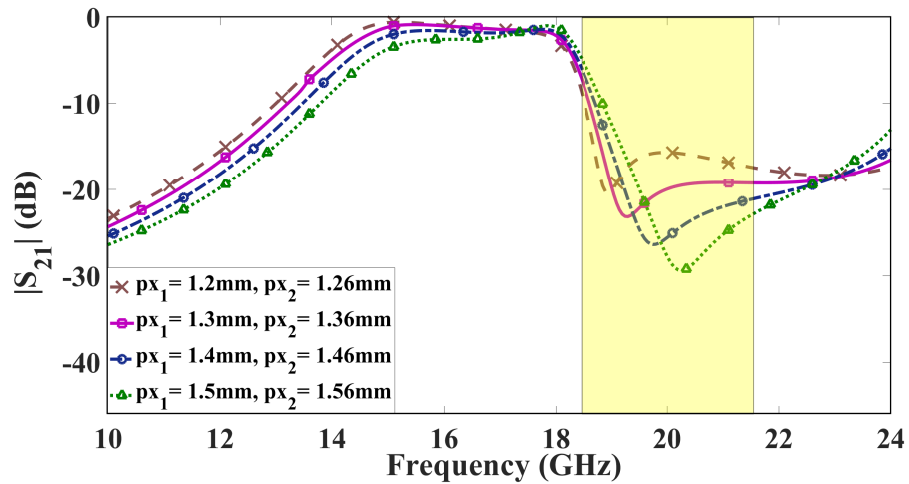
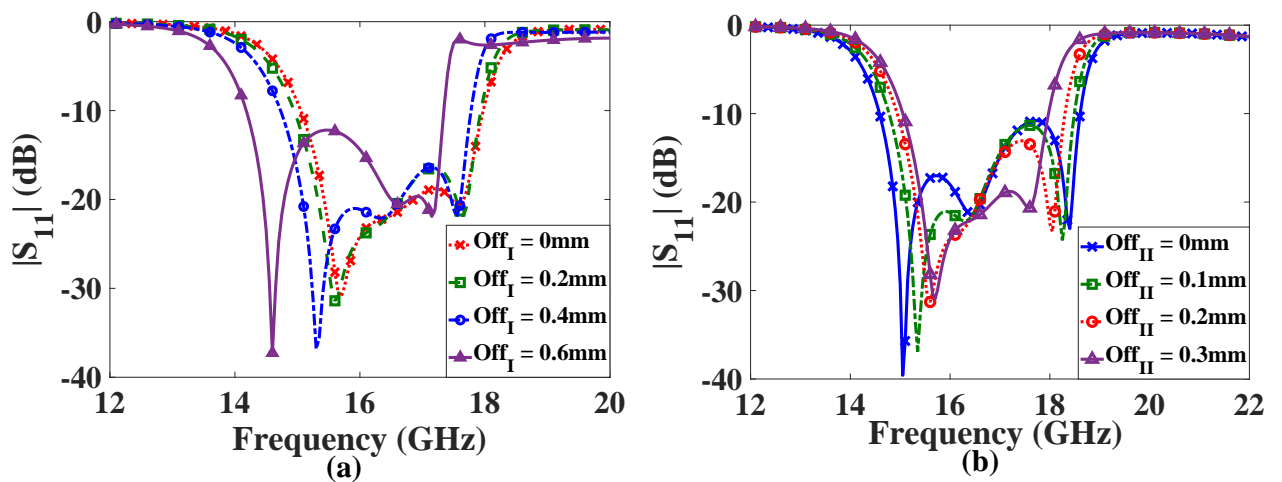


Figure 3.46 : Study of proposed triple-mode SICR based bandpass filter with variation of transmission zero with offset of SICR



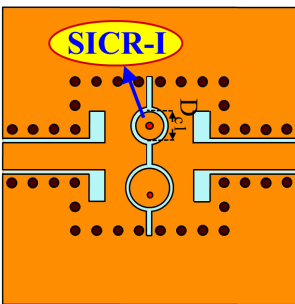
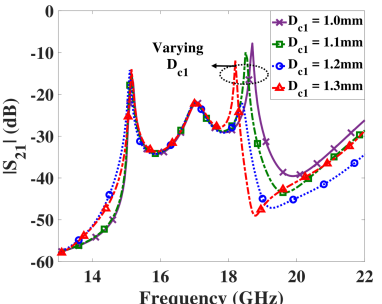
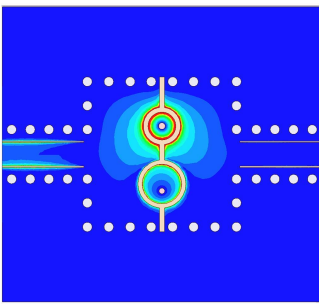
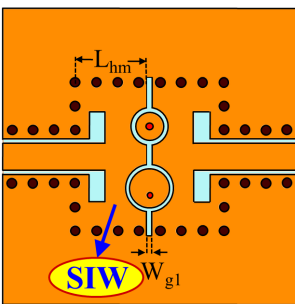
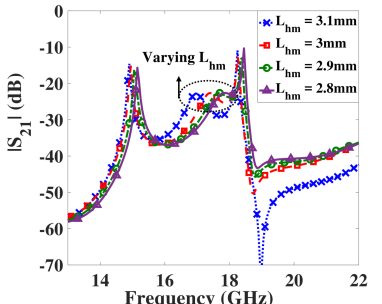
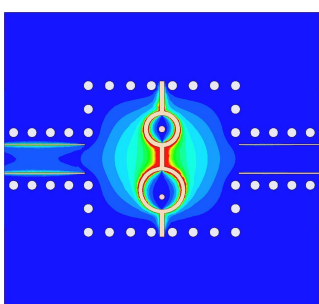
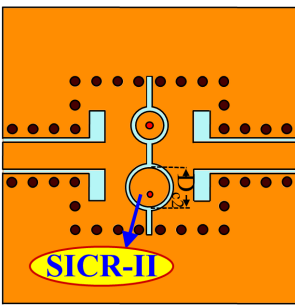
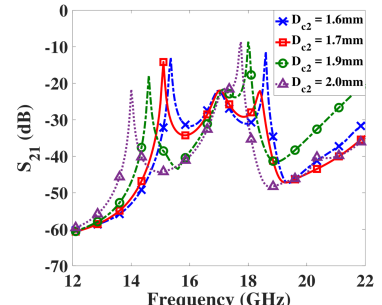
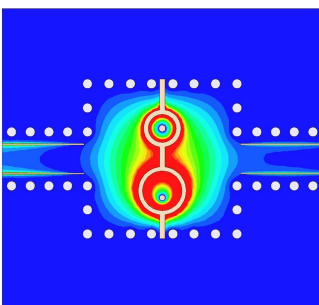
to the ground plane through a circular patch of radius R_b and gap G_{bn} (where $n = 1$) is modeled as a series LC circuit (L_v and C_v) in Fig 3.50 . Effective inductance contributed by the metallic via (3.4) can be approximated using [104]

$$L_v = 5.08h \left[\ln \left(\frac{4h}{D_q} \right) + 1 \right] \quad (3.4)$$

Using the above equation the inductance offered by the via is computed as 0.61 nH. A band reject response at 28.5 GHz is affirmed through Ansys HFSS for via with diameter D_q that is directly connected to signal line of GCPW and capacitively coupled to bottom ground plane through gap (G_{bn}). The capacitance C_v of the series LC circuit is determined as 0.05 pF by equation (3.5).

$$C_v = \frac{1}{\omega_r^2 L_v} \quad (3.5)$$

Table 3.6 : Varying D_{c1} (c) Varying L_{hm} (d) Varying D_{c2} , (for fixed slot slot dimension $W_{g1} = 0.21\text{mm}$)

	Layout	S-parameters	E-field
(a) Varying D_{c1}			
(b) Varying L_{hm}			
(c) Varying D_{c2}			

To attain better flexibility in tuning the transmission zero the via is connected to the signal line of GCPW through a metallic strip of length L_{in} (where $n = 1$). With metal strip of length $L_{t1} = 2.71\text{mm}$, the transmission zero shifts from 28.5 GHz to 11.6 GHz. The ABCD matrix [80] of the circuit model depicting plated via connected to metal strip (blue color dashed box in Fig. 3.50) is given as 3.6.

$$ABCD_{ckt} = \begin{bmatrix} 1 & 0 \\ Y_{in} & 1 \end{bmatrix} \quad (3.6a)$$

$$Y_{in} = \left[\left(\frac{1}{j\omega C_v} + j\omega L_v \right) + \left(\frac{1}{j\omega C_s} \parallel j\omega L_s \right) \right]^{-1} \quad (3.6b)$$

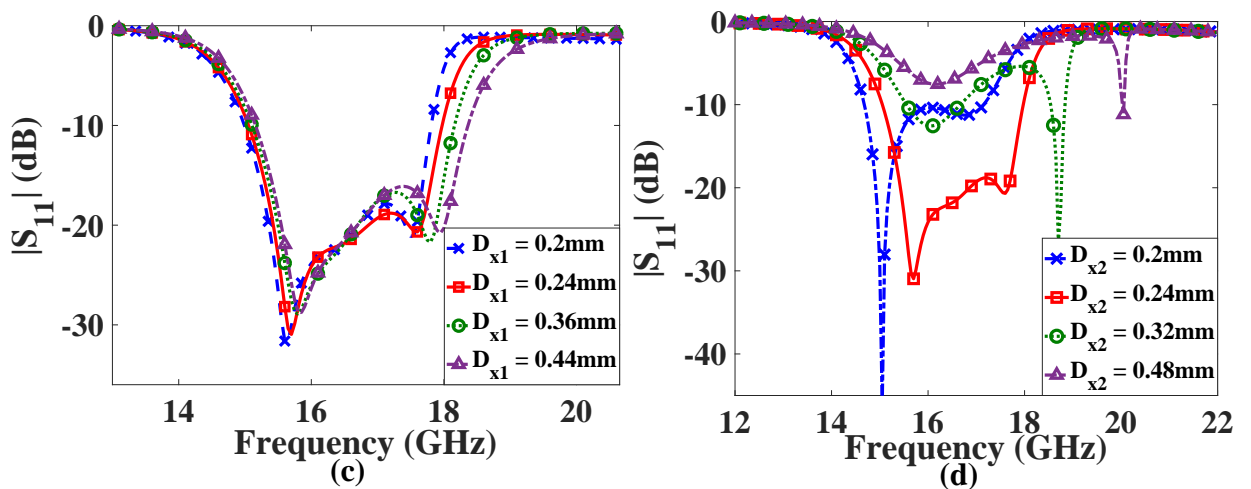


Figure 3.47: Varying offset of inner conductor in (a) SICR-I (b) SICR-II, Varying diameter of inner conductor in (c) SICR-I (d) SICR-II

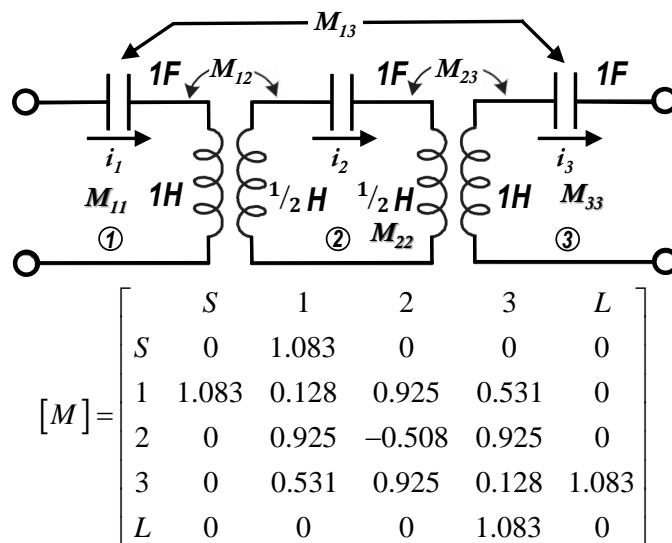


Figure 3.48: SICR filter C: Equivalent circuit model synthesized using coupling matrix

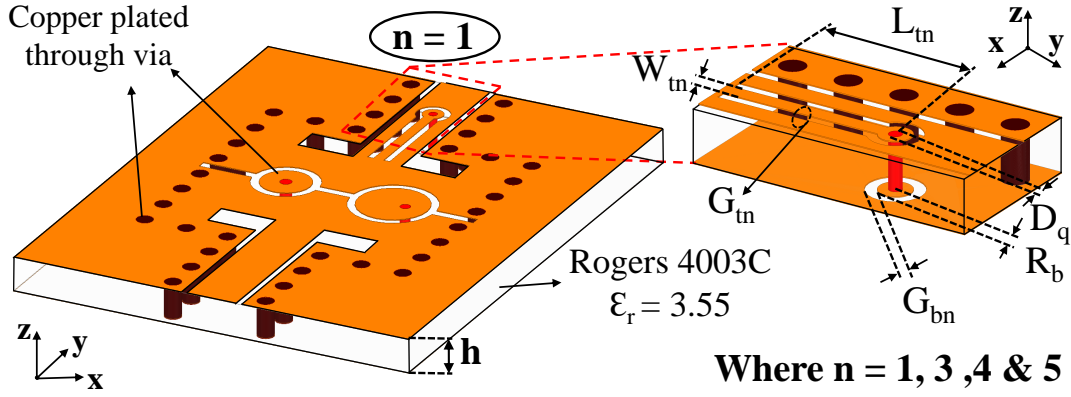


Figure 3.49 : Layout of proposed SICR Filter D: $D_q = 0.2\text{mm}$, $G_{b1} = 0.17\text{mm}$, $G_{t1} = 0.15\text{mm}$, $h = 0.8\text{mm}$, $L_{t1} = 2.7\text{mm}$, $R_b = 0.25\text{mm}$, $W_{t1} = 0.25\text{mm}$.

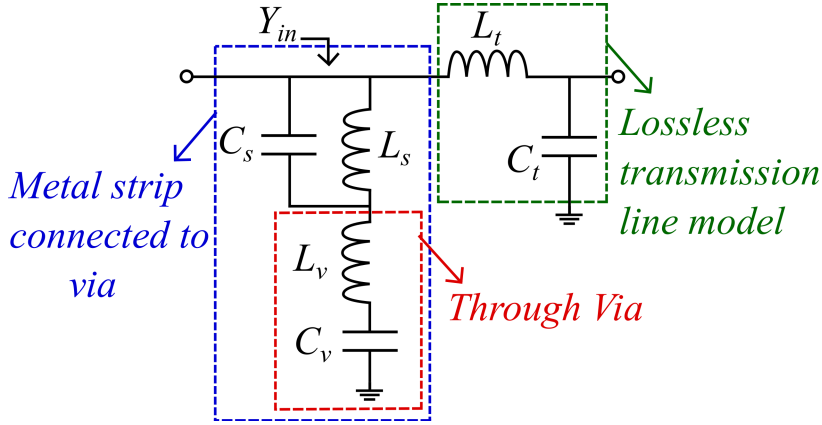


Figure 3.50 : Equivalent circuit model of the proposed bandstop resonator.

The ABCD matrix of a two-port network is converted into S-parameters [125] using 3.7.

$$S_{11} = \frac{A + B/Z_0 - CZ_0 - D}{A + B/Z_0 + CZ_0 + D} \quad (3.7a)$$

$$S_{21} = \frac{2}{A + B/Z_0 + CZ_0 + D} \quad (3.7b)$$

Using S-parameters obtained from Ansys HFSS for the full-wave simulation model, (4a) and (4b) result in two equations in terms of L_s and C_s . From MATLAB the values of L_s and C_s are determined as 2.91 nH and 0.0052 pF respectively. In Fig. 3.50, the circuit parameters $L_t = 0.18\text{nH}$, $C_t = 0.07\text{pF}$ of a lossless transmission line model are obtained by extracting the telegrapher's equation parameters as described in [106]. The ABCD matrix of transmission line model is given by 3.8

$$ABCD_{TL} = \begin{bmatrix} 1 & j\omega L_t \\ 0 & 1 \end{bmatrix} \begin{bmatrix} 1 & 0 \\ j\omega C_t & 1 \end{bmatrix} \quad (3.8)$$

The theoretical S-parameters of proposed bandstop resonator are determined from the product of ABCD matrix in 3.6 and 3.8. The theoretical, circuit simulated and full-wave simulated results as shown in Fig. 3.51(a) are in good agreement with each other. the thesis. The synthesized

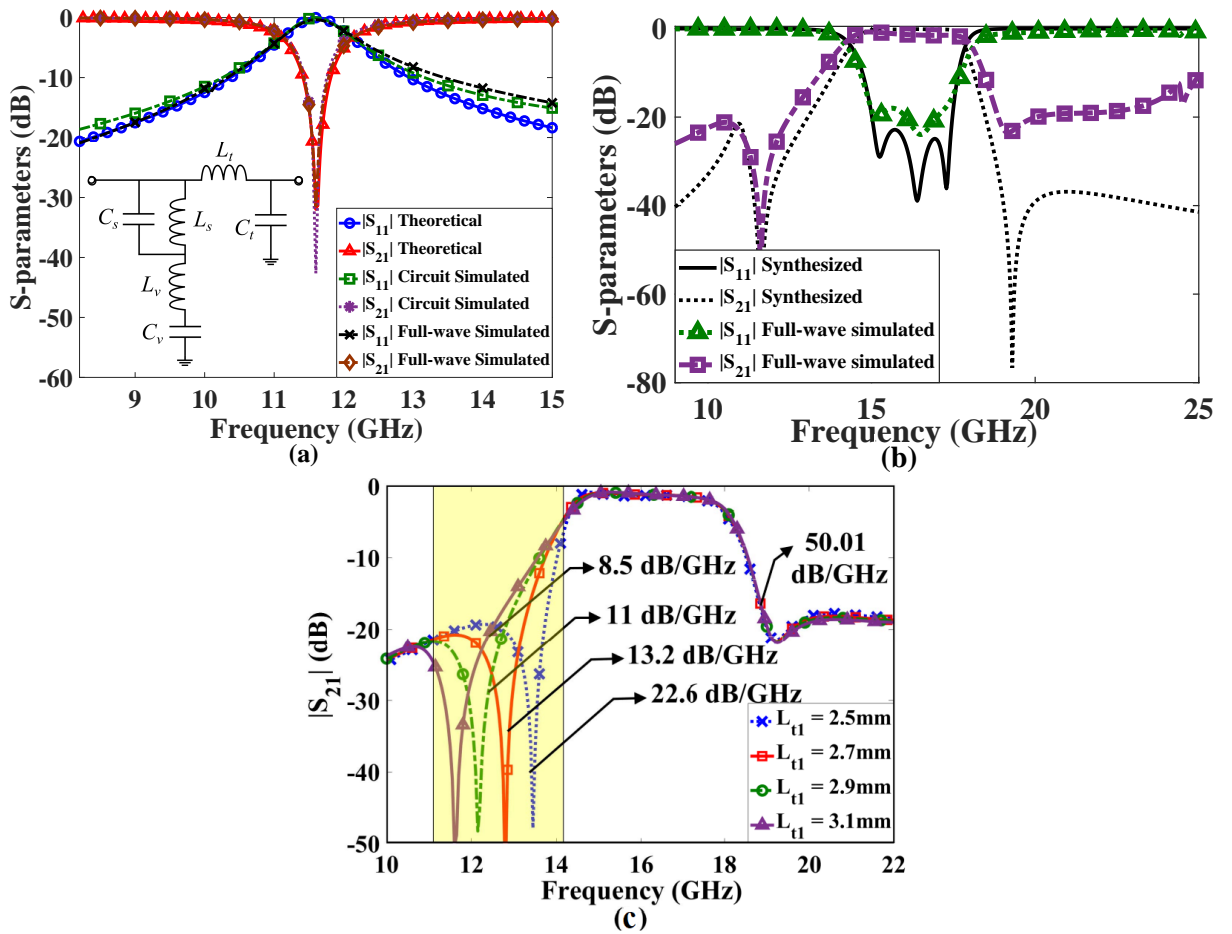


Figure 3.51: Design of Filter D (a) Equivalent circuit model of proposed bandstop resonator (b) Theoretically synthesized response of Filter D (c) Flexible transmission zero shown through full-wave simulation.

response of filter B is computed in MATLAB by cascading ABCD matrices of Filter D and the proposed bandstop resonator as shown in Fig. 3.51(a). Further, the full-wave simulated results of final Filter D demonstrates independent tuning of transmission zero by varying L_{t1} as shown in Fig. 3.51 (b). The proposed topology replicates a partial height via with a much simpler fabrication process to generate a flexible transmission zero on the lower edge of passband in Filter D. Here, flexible means the ability to easily modify the design to achieve the required specification. Though several novel coupling schemes have been reported in the past to introduce a transmission zero, their implementation is however limited by filter topology. This brings to the need of proposed technique where transmission zero is induced without changing the filter topology or inter-resonator coupling.

3.5.3 Modeling of SICR based bandpass filter with enhanced out of band rejection: Filter E

The flexibility of proposed planar bandstop resonator explored in the previous section is utilized to design Filter E by embedding three more such resonators on the feed line to improve the out of band rejection of the filter. The geometrical layout of Filter E with dimensions is shown in Fig. 3.52. The proposed configuration provides two degrees of freedom in adjusting the position of each transmission zero (T_{zn}) independently by varying length of metal strip (L_{tn}) & gap (G_{bn}) as shown in Fig. 3.53 (where $n = 1, 3, 4$ & 5). Moreover, this topology is better suited to implement at

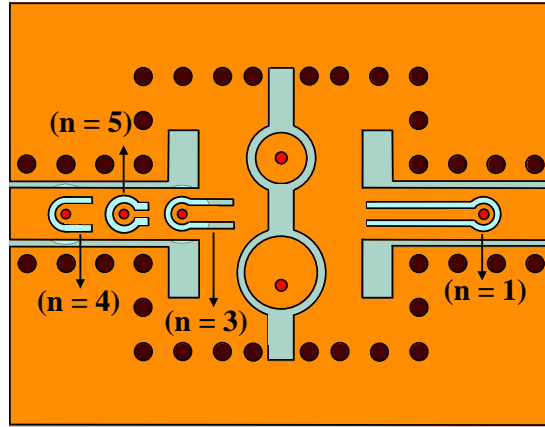


Figure 3.52 : Layout of SICR based bandpass filter (Filter E) with dimensions: $G_{b3} = 0.42\text{mm}$, $G_{b4} = 0.45\text{mm}$, $G_{b5} = 0.17\text{mm}$, $G_{t1} = G_{t3} = G_{t4} = 0.15\text{mm}$, $G_{t5} = 0.2\text{mm}$, $L_{t3} = 1.21\text{mm}$, $L_{t4} = 0.62\text{mm}$, $L_{t5} = 0.58\text{mm}$, $W_{g1} = 0.6\text{mm}$, $W_{t3} = 0.4\text{mm}$, $W_{t4} = 0.5\text{mm}$, $W_{t5} = 0.15\text{mm}$.

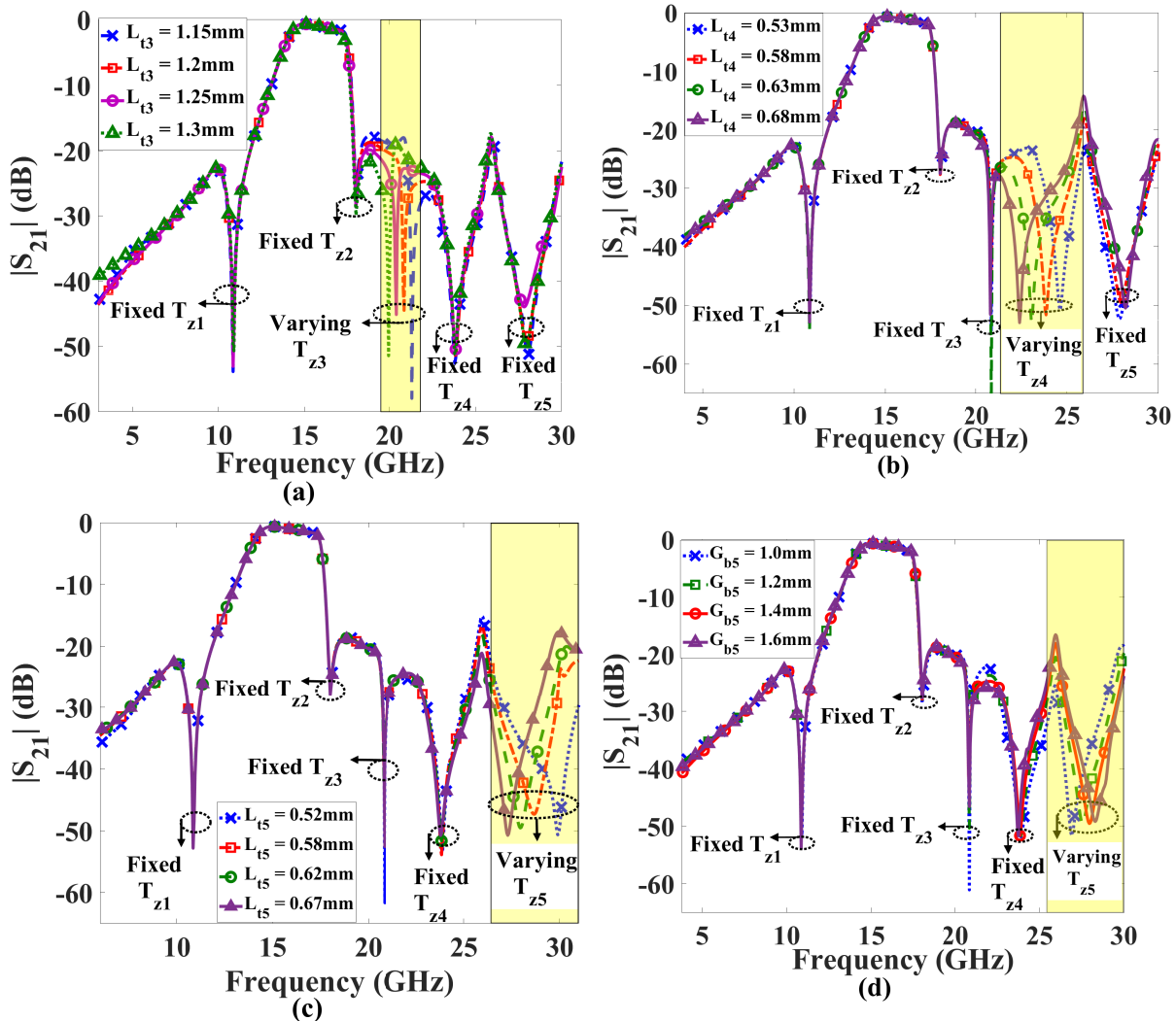


Figure 3.53 : Flexibility in controlling the position of each individual transmission zero with variation in (a) L_{t3} (b) L_{t4} (c) L_{t5} (d) G_{b5} .

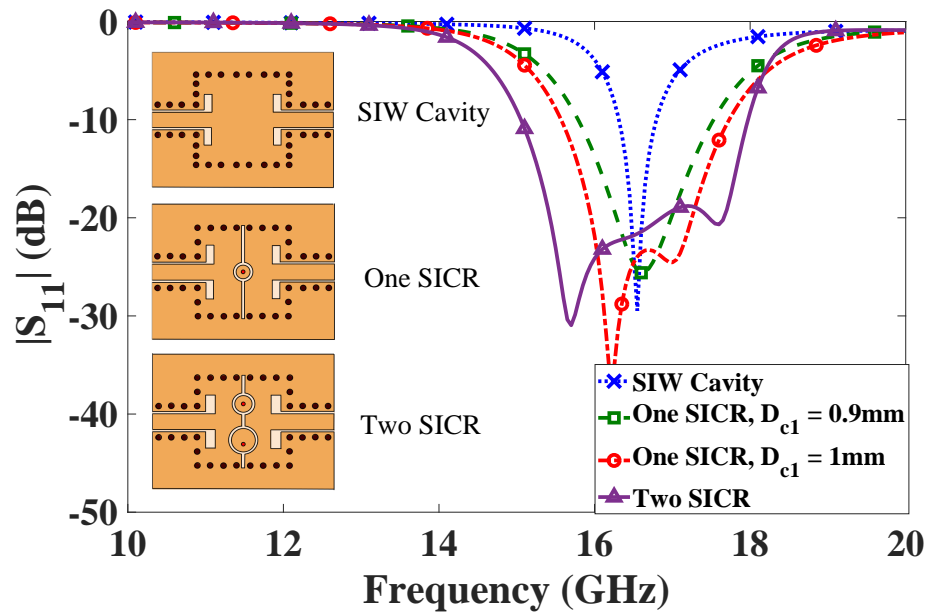


Figure 3.54 : Study on bandwidth enhancement and adjustability based on number of embedded SICR and variation in D_{c1} for the proposed filter.

higher frequencies as it is less prone to radiation loss.

3.5.4 Comments on bandwidth control

Conventionally to improve the bandwidth of bandpass Filter cascading multiple cavities is considered as a popular technique with the inherent drawback of large size. A conventional SIW square cavity exhibits a 3-dB FBW (fractional bandwidth) of 8.3%. In the proposed technique, by embedding a single external SICR the FBW of a narrow band SIW cavity is improved. The bandwidth can be adjusted by varying the diameter of the capacitive patch (D_{c1}) connected to central via as shown in Fig. 3.54. However, the maximum achievable FBW by using one SICR

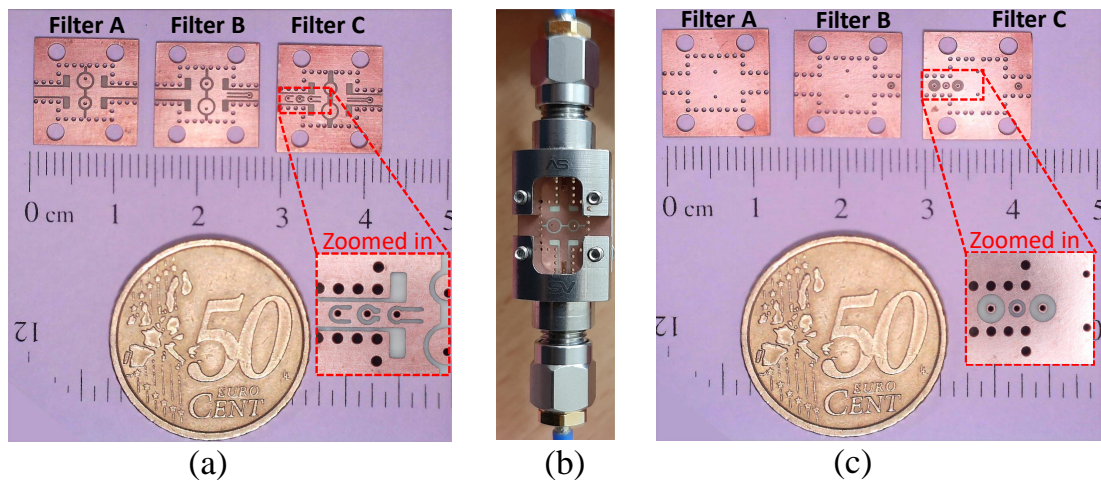


Figure 3.55 : Photograph of the three experimental prototypes (a) Top view (b) Fabricated prototype with connectors (c) Bottom view.

Table 3.7 : Comparison of proposed BPF with previously reported BPF's

Ref	Tech.	f_o	Order	$ S_{21} $ (dB)	Size (λ_g^2)	Layers	Bandwidth (%)	Structure	Flexibility ^Δ	# Tz/s
	Microstrip	13.2	5	1.75	0.11	1	7.58	semi-open	No	5
	Microstrip	13.31	5	2.1	0.12	1	4.70	semi-open	No	0
[21]	Microstrip	13.325	5	1.78	0.06	1	7.50	semi-open	No	0
	SIW	13.06	5	1.96	1.48	1	10.53	shielded	No	0
[22]	MS	15.86	2	2.5	0.126	1	36	semi-open	No	1
[74]	LTC	14.52	2	3.27	0.37	8	7.57	packaged	No	0
[98]	LCP	17.2	3	2.9	0.28	3	17.3	-	No	2
[99]	SIW	12.6	6	1.4	-	1	10	shielded	No	2
[100]	SIW	13	2	1.7	0.71	2	4.6	shielded	No	0
	SIW	13.2	2	1.5	0.71	2	4.5	shielded	No	4
[101]	SIW	13.53	3	1.12	0.71	2	3.91	shielded	Yes	3
[92]	SICL	13.83	2	1.18	0.31	2	2.6	shielded	No	2
[79]	ESICL	15	4	1.59	2.85	5	2.93	shielded	No	0
[107]	SIW*	9.8	3	1.7	0.54	1	5	shielded	No	0
[108]	SIW*	5.75	3	3.6	0.74	1	1.8	shielded	No	2
[109]	SIW*	8	2	1.7	0.18	1	20	shielded	Yes	2
	SICR ^C	16.38	3	1.21	0.43	1	24.66	shielded	Yes	1
TW	SICR ^D	16.14	3	1.67	0.48	1	24.60	shielded	Yes	2
	SICR ^E	15.73	3	1.71	0.5	1	23.01	shielded	Yes	5

TW: This work, *: Coaxial SIW, Δ: Flexibility to adjust Tz and BW

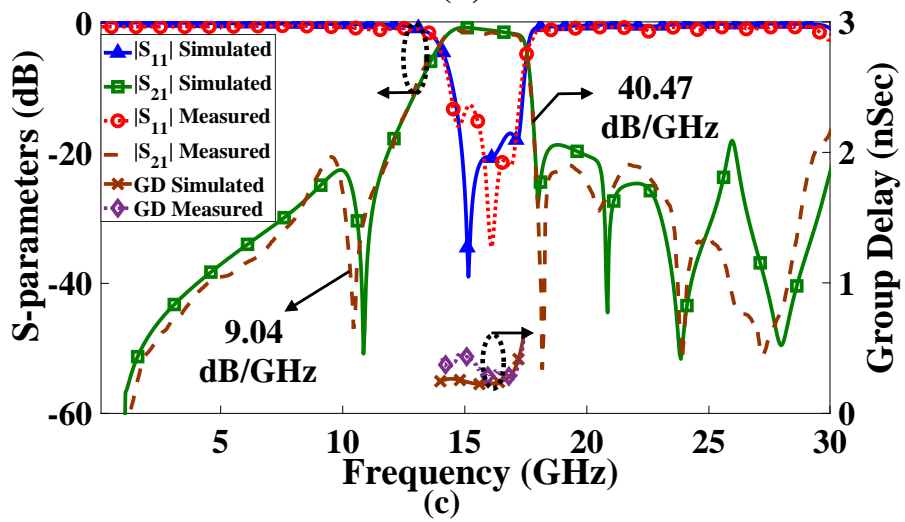
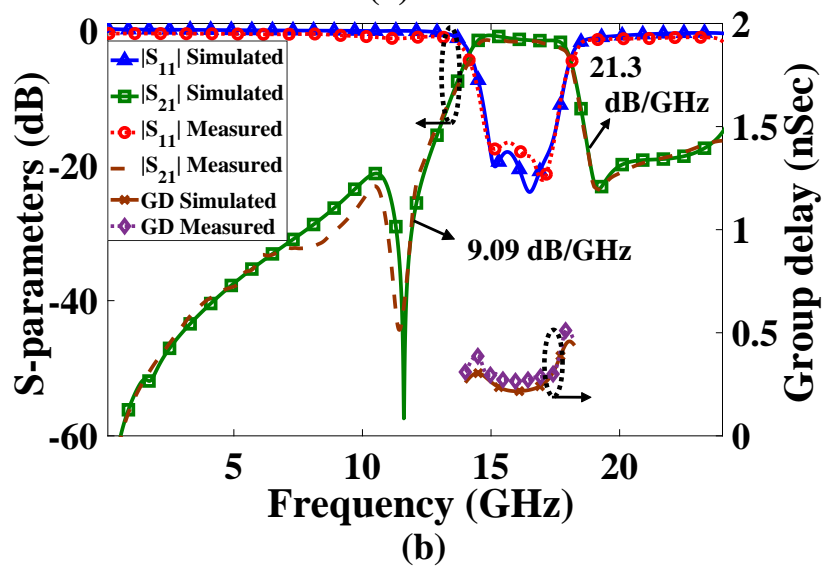
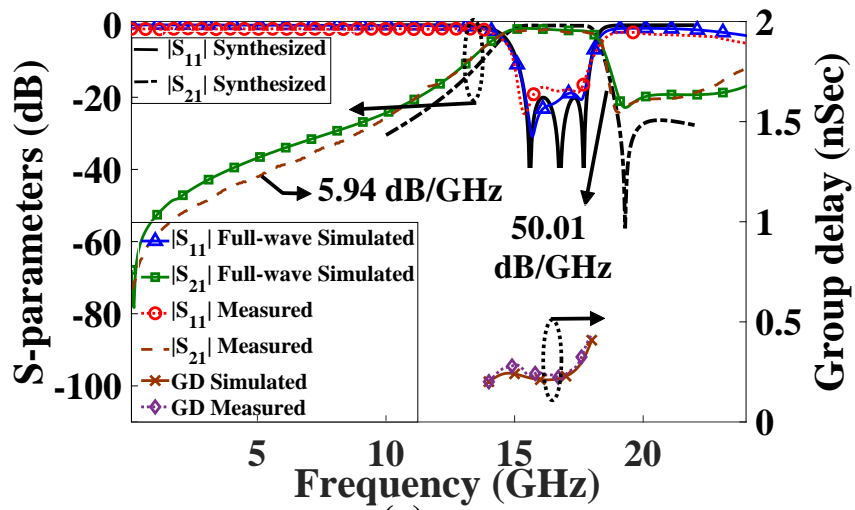


Figure 3.56 : Comparison between full-wave simulated and measured results (a) Filter C (b) Filter D (c) Filter E.

(D_{c1}) is 18.4%. To further increase the FBW, two SICR are embedded in the cavity to achieve a maximum FBW of 24.66% as shown in Fig. 3.54. By adjusting the diameter of the capacitive patch (D_{c1} , D_{c2}) connected to via, the FBW can be adjusted as per user requirement between 8.3% to 24.66% without changing the size of the cavity.

3.5.5 Results and Discussion

To validate the proposed filter synthesis, three prototypes have been manufactured. The SICR based filters are developed on a single layered Rogers 4003C substrate ($\epsilon_r = 3.55$, $\tan\delta = 0.0014$) of thickness 0.8 mm using low cost PCB fabrication technology. The photograph of the fabricated prototype depicting its top and bottom view with connectors are shown in Fig. 3.55. SV Microwave solderless end launchers (SF2921-61450/ SF1621-60036) have been utilized to facilitate the testing of proposed experimental prototypes. The full-wave S-parameters computed using Ansys HFSS are affirmed by recording the S-parameters of proposed prototypes using Agilent N5234A (10 MHz to 43.5GHz) vector network analyzer as shown in Fig. 3.56. In Fig. 3.56(a), measured results of Filter C demonstrates an insertion loss of 1.2 dB at the center frequency 16.38 GHz with a transmission zero on the upper side of passband. The proposed filter exhibits a fractional bandwidth of 24.66% with 3-dB passband of 4.04 GHz centered at 16.38 GHz. In order to improve the selectivity on the lower edge of passband Filter D has been proposed. In Fig. 3.56(b), a transmission zero on lower side of the passband at 11.42 GHz is produced due to the bandstop resonator on GCPW feed line in Filter D. Further the proposed filter maintains almost same bandwidth as Filter C. The measured results of Filter E in Fig. 3.56(c) indicate an insertion loss of 1.71 dB at center frequency 15.73 GHz and features 5 transmission zeros at 10.44 GHz, 18.17 GHz, 20.54 GHz, 23.9 GHz and 27.22 GHz which can be independently tuned by varying L_{mn} and G_{bn} (where $n = 1, 3, 4$ and 5). Further the measured peak to peak group delay for all the three experimental prototypes are within 0.28 nsec and their roll-off rates are indicated in Fig. 3.56. The proposed SICR based filters are compared with current state of the art bandpass filter (BPF) in Table 3.7. It provides better bandwidth than SIW based filters, lower insertion loss than microstrip based filters and is easier and economical to manufacture than other substrate integrated technologies. The prominent features of proposed SICR bandpass filters are discussed in brief as below:

1. **Enhanced-bandwidth:** The proposed K_u -band BPF enhances the bandwidth of a conventional SIW cavity by combining SIW mode & two TEM coaxial modes of embedded SICR to achieve a FBW of 24.66%, i.e 4.04 GHz passband centered at 16.38 GHz.
2. **Improved selectivity and out of band performance:** A novel design technique to improve the selectivity and out of band rejection of the filter is developed in this work. All the 5 transmission zeros of the filter demonstrate high degree of flexibility to be adjusted as per user requirement.
3. **Smaller than SIW:** A triple-mode filter is realized using single layered substrate within a compact size of $0.43\lambda_g^2$. The proposed filter uses a SIW based cavity that is 13% smaller than conventional SIW cavity & offers around thrice FBW of an SIW cavity.
4. **Adjustable bandwidth:** The proposed technique developed from a narrow band SIW cavity demonstrates adjustable bandwidth by use of external SICR's. The bandwidth can be chosen as per user requirement by varying the number of SICR resonators and radius of capacitive patch (D_{c1} , D_{c2}) connected to the via.

3.6 CONCLUSIONS

Several novel design techniques to improve the performance of the microwave and millimeter-wave bandpass filters have been proposed in this chapter. The proposed designs

Table 3.8 : Comparison between theoretically synthesized and full-wave simulated results of the proposed bandpass filters

Chapter no.	Work	Simulation	Center frequency (GHz)	$ S_{11} $ (dB)	$ S_{21} $ (dB)
3.1	Via perturbed bandpass filter	Equivalent Circuit	13.89	23.08	0.02
		Full-wave Simulation	13.89	21.05	0.79
3.2	SICL cavity filter	Equivalent Circuit	28.15	20.14	0.23
		Full-wave Simulation	28.15	22.92	0.42
3.4	Quarter-mode SICL cavity filter	Equivalent Circuit	12.59	19.85	0.14
		Full-wave Simulation	12.59	20.32	0.22
3.5	SICR Bandpass filter C	Equivalent Circuit	16.38	22.08	0.12
		Full-wave Simulation	16.38	22.05	1.19
3.5	SICR Bandpass filter D	Equivalent Circuit	16.12	20.67	0.15
		Full-wave Simulation	16.12	28.11	1.35

support wide bandwidth, high selectivity, good out of band rejection in a compact form factor.

First, A novel perturbation technique for a ring resonator implemented in SICL technology has been utilised to design a completely shielded dual-mode bandpass filter with low insertion loss for K_u -band in the fourth design. The outer conductor formed by lateral vias in SICL is utilised to excite the degenerate modes. Further, length and inset of perturbation formed by lateral vias to control the coupling between orthogonal modes and attenuation poles has been studied. The experimentally tested prototype demonstrated a low insertion loss of 1.18 dB with 2.6% FBW centred at 13.83 GHz. The proposed perturbation technique motivates design and development of a new class of microwave and millimeter-wave components in the shielded and self-packaged SICL technology.

The design and detailed analysis of a dual-mode Substrate Integrated Coaxial Line (SICL) bandpass filter operating at 28 GHz has been demonstrated. The dual-mode response in the proposed filter has been achieved by exciting the degenerate modes in the square-shaped inner conductor of the SICL section. Cross-shaped slots of unequal widths and lengths are utilized to facilitate the coupling according to the generated coupling matrix between higher order modes to attain a dual mode response at 27.365 GHz. The proposed SICL cavity occupies only 53.2% area as compared to a SIW cavity. The electromagnetic shielding capability of the proposed bandpass filter along with its size reduction makes it a highly desirable candidate for millimeter-wave applications.

In the third design, analysis of two second order SICL based bandpass filters operating at 28 GHz with multiple transmission zeros is demonstrated with better size reduction. A SICL cavity comprising of a L-bend line is analyzed and its half mode counterpart is conceived. A mode chart to determine the resonant frequency of fundamental as well as higher order modes of the proposed SICL cavity and its half mode has been developed. In the designed filter the frequency selectivity is enhanced by a pair of transmission zeros on each lower and upper side of the passband. In addition, a new SICL filter integrated with band-reject resonators for extended out of band response possessing controllable transmission zeros is devised with simple design procedure. The proposed SICL filters (*filters A and B*) exhibit a 14.21% & 11.64% 3-dB fractional bandwidth respectively, with good out of band performance in a compact size. The superior integration capability with planar circuits and broad monomode TEM operation advocates the utilization of proposed SICL based bandpass filters in millimeter-wave range.

The third design leverages the low-loss, shielded and wideband transmission properties of SICL to implement a dual-mode SICL based dual-bandpass filter with widely spaced passbands located in X and K-band. Flexible filter response owing to simple topology for single-band and dual-band operation has been analyzed. Use of SICL as planar guiding media for filter design aids in building a RF-front end architecture where small form factor is preferred for installation in modern hand-held devices and access points.

Finally, a single layer implementation of a coaxial resonator and the analysis of versatile bandpass filters with enhanced bandwidth and transmission zeros exhibiting high degree flexibility to improve selectivity as well as out of band rejection has been demonstrated. Further, the adjustable bandwidth and independently tunable transmission zeros to design as per user requirement for K_u -band are the notable features of proposed work. Three experimental prototypes are developed and tested to show a FBW better than 23% in a size less than $0.5\lambda_g^2$. The proposed technique can be extended to develop passive and active microwave/millimeter-wave components with inherent filtering characteristics. In Table 3.8, a consolidated comparison between theoretically synthesized and full-wave simulated results of the SICL based bandpass filters in Chapter-3 is shown.

...